

HYDROGEN STORAGE CAPACITY OF NANOSYSTEMS:
MOLECULAR –DYNAMICS SIMULATIONS

A THESIS SUBMITTED TO
THE GRADUATE SCHOOL OF NATURAL AND APPLIED SCIENCES
OF
MIDDLE EAST TECHNICAL UNIVERSITY

BY

AYTUN KOYUNCULAR ONAY

IN PARTIAL FULLFILLMENT OF THE REQUIREMENTS
FOR
THE DEGREE OF MASTER OF SCIENCE
IN
PHYSICS

MAY 2008

Approval of the thesis:

**HYDROGEN STORAGE CAPACITY OF NANOSYSTEMS:
MOLECULAR –DYNAMICS SIMULATIONS**

submitted by **Aytun Koyuncular Onay** in partial fulfillment of the requirements for the degree of **Master of Science in Department, Middle East Technical University** by,

Prof. Dr. Canan Özgen _____
Dean, Graduate School of **Natural and Applied Sciences**

Prof. Dr. Sinan Bilikmen _____
Head of Department, **Physics Department**

Prof. Dr. Şakir Erkoç _____
Supervisor, **Physics Department**

Examining Committee Members:

Prof. Dr. Ramazan Sever _____
Physics Dept., METU

Prof. Dr. Şakir Erkoç _____
Physics Dept.,

Prof. Dr. Lemi Türker _____
Chemistry Dept., METU

Prof. Dr. Demet Gülen _____
Physics Dept., METU

Assist. Prof. Dr. Hande Üstünel _____
Physics Dept., METU

Date: 27.05.2008

“I hereby declare that all information in this document has been obtained and presented in accordance with academic rules and ethical conduct. I also declare that, as required by these rules and conduct, I have fully cited and referenced all material and results that are not original to the this work.”

Name Surname : AYTUN KOYUNCULAR ONAY

Signature :

ABSTRACT

HYDROGEN STORAGE CAPACITY OF NANOSYSTEMS: MOLECULAR –DYNAMICS SIMULATIONS

Koyuncular Onay, Aytun

M.S., Department of Physics
Supervisor : Prof. Dr. Şakir Erkoç

May 2008, 70 pages.

In recent decades, tremendous efforts have been made to obtain high hydrogen storage capacity in a stable configuration. In the literature there are plenty of experimental works investigating different materials for hydrogen storage and their storage values. In the first part of this thesis the available literature data have been collected and tabulated. In addition to the literature survey the hydrogen storage capacity of carbon nanotubes and carbon nanotubes doped with boron nitride (CBN nanotubes) with different chirality have been investigated by performing quantum chemical methods at semiempirical and DFT levels of calculations. It has been found that boron nitride doping increases the hydrogen storage capacity of carbon nanotubes. Single wall carbon nanotubes (SWNT) can be thought as formed by warping a single graphitic layer into a cylindrical object. SWNTs attract much attention because they have unique electronic properties,

very strong structure and high elastic moduli. The systems under study include the structures C(4,4), H₂@C(4,4), C(7,0), C(4,0), and the BN doped C(4,4), H₂@C(4,4), 2H₂@C(4,4), C(7,0), H₂@C(7,0), 2H₂@C(7,0). Also, we have investigated adsorption and desorption of hydrogen molecules on BN doped coronene models by means of theoretical calculations.

Keywords: Hydrogen storage, carbon nanotubes, quantum chemical methods

ÖZ

NANOSİSTEMLERİN HİDROJEN DEPOLAMA KAPASİTESİ: MOLECULAR –DİNAMİK SİMULASYONLARI

Koyuncular Onay, Aytun

Yüksek Lisans, Fizik Bölümü
Tez Danışmanı : Prof. Dr. Şakir Erkoç

Mayıs 2008, 70 sayfa.

Son on yıldır, kararlı bir yapıda, hidrojen depolama kapasitesini arttırmak amacıyla çok sayıda çalışmalar yapılmaktadır. Literatür çalışması içerisinde, bol miktarda farklı materyallerin üzerinde yapılan deneysel çalışmaların sonucunda elde edilen hidrojen depolama değerleri yer almaktadır. Tez çalışmasının ilk kısmında mevcut literatür verileri toplanmış ve bunlar tablo halinde sırasıyla verilmiştir. Buna ek olarak, farklı çap ve uzunluktaki karbon nanotüplerde ve boron-nitrat katkılı karbon nanotüplerde hidrojen depolama kapasitesi, kuantum kimyasal metotlardan yarı deneysel ve DFT yöntemleri kullanılarak araştırıldı. Bu çalışmanın sonucunda boron-nitrat katkısının karbon nanotüplerde hidrojen depolama kapasitesini arttırdığı gözlemlendi. Tek duvarlı karbon nanotüpler bir grafit tabakasının silindirik bir şekilde yuvarlanması olarak düşünülebilir. Tek duvarlı

karbon nanotüplerin büyük ilgi görmesinin nedeni elektronik özellikleri, güçlü yapısı ve yüksek esneklik katsayısıdır. Bu tez çalışmasında üzerinde durulan nanoyapılar C(4,4), H₂@C(4,4), C(7,0), C(4,0), ve BN katkılı C(4,4), H₂@C(4,4), 2H₂@C(4,4), C(7,0), H₂@C(7,0), 2H₂@C(7,0), ve C(4,4)'dir. Son olarak BN katkılı koronen modelinin hidrojen depolama ve geri bırakma özellikleri teorik hesaplamalar yardımıyla araştırıldı ve sonuçlar yorumlandı.

Anahtar sözcükler: Hidrojen depolama, karbon nanotüpler, quantum kimyasal metotlar.

To My Lovely Husband, Mother and Father

ACKNOWLEDGEMENTS

I would like to thank to my supervisor Prof. Dr. Şakir Erkoç for his patience and encouragement and supervision throughout this study.

I am deeply grateful to Deniz Çalışır Tekin, Emre Taşçı, Nazım Dugan, Dr. Hande Üstünel for their help, guidance and encouragement in this study.

I would also like to thank everyone in our group in METU for their friendship and help, especially Olcay Üzengi Aktürk, İpek Güler and my lab friends Rengin Peköz, O. Barış Malcıoğlu for their sincere friendship.

I would like to send my appreciation to my gratitude to dear Melih Onay for his endless patience, support and love.

I am grateful to both my father İ. Hüsnü Koyuncular and my mother Letiman Koyuncular for their encouragement and trust.

I want to express my sincere gratitude to TÜBİTAK for financial support to my thesis through the project TUBITAK-TBAG-107T142 and to thank METU through the project METU-BAP-2006-07-02-00-01 respectively.

TABLES OF CONTENTS

ABSTRACT.....	iv
ÖZ.....	vi
ACKNOWLEDGEMENTS.....	ix
TABLE OF CONTENTS.....	x
LIST OF TABLES.....	xii
LIST OF FIGURES.....	xv
CHAPTER	
1. INTRODUCTION	1
1.1. Introduction.....	1
1.2. Hydrogen Storage Methods.....	3
1.2.1. Physisorption.....	4
1.2.1.1 Properties of Absorbing Hydrogen with Physisorption.....	5
1.3. Molecular Dynamics Simulations of H ₂ Storage in Carbon Nanotubes and CBN Nanotubes	6
1.4. Molecular Dynamics Simulations of H ₂ Storage in BN Doped Coronene Model.....	7
2. MATERIALS FOR HYDROGEN STORAGE AND THEIR CAPACITY.....	8
2.1 Introduction.....	8
2.2 Tables of commercial materials for hydrogen storage.....	8

3. METHOD OF CALCULATION.....	25
3.1.1. Computational Methods.....	25
3.1.2. DFT Studies for Carbon Nanotubes and CBN Nanotubes.....	26
3.1.3. Molecular Mechanics Method Studies for Carbon Nanotubes and CBN Nanotubes.....	27
3.1.4. Molecular Dynamics Simulation Studies for Carbon Nanotubes and CBN Nanotubes.....	28
3.2.1. DFT Studies for BN Doped Coronene Model.....	28
3.2.2. Molecular Dynamics Simulation Studies for BN Doped Coronene Model.....	29
4. RESULTS AND DISCUSSIONS.....	30
4.1.1. DFT Study Results for Carbon Nanotubes and CBN Nanotubes.....	30
4.1.2. Molecular Mechanics Method Study Results for Carbon Nanotubes and CBN Nanotubes.....	36
4.1.3. Molecular Dynamics Simulation Study Results for Carbon Nanotubes and CBN Nanotubes.....	37
4.2.1. DFT Study Results for BN Doped Coronene Model	47
4.2.2. Molecular Dynamics Simulation Study Results for BN Doped Coronene Model.....	48
5. CONCLUSION.....	56
REFERENCES.....	58

LIST OF TABLES

TABLES

Table 1.1	Properties of hydrogen.....	2
Table 1.2	The theoretical hydrogen storage capacity formula.....	4
Table 2.1a	MS: material structure; C: catalysts; PAM: purification activation method; T: temperature; P: pressure; HSC: hydrogen storage capacity; R: references.....	9
Table 2.1b	MS: material structure; C: catalysts; PAM: purification activation method; T: temperature; P: pressure; HSC: hydrogen storage capacity; R: references.....	10
Table 2.2a	MS: material structure; C: catalysts; PAM: purification activation method; T: temperature; P: pressure; HSC: hydrogen storage capacity; R: references.....	11
Table 2.2b	MS: material structure; C: catalysts; PAM: purification activation method; T: temperature; P: pressure; HSC: hydrogen storage capacity; R: references.....	12
Table 2.3	MS: material structure; C: catalysts; PAM: purification activation method; T: temperature; P: pressure; HSC: hydrogen storage capacity; R: references.....	13
Table 2.4	MS: material structure; EC: experimental conditions; T: temperature; P: pressure; HSC: hydrogen storage capacity; R: references.....	14
Table 2.5	MS: material structure; T: temperature; P: pressure; HSC: hydrogen storage capacity; R: references.....	16
Table 2.6	MS: material structure; T: temperature; P: pressure; HSC: hydrogen storage capacity; R: references.....	17

Table 2.7 MS: material structure; T: temperature; P: pressure; S: samples ; R: references.....	18
Table 2.8 MS: material structure; T: temperature; P: pressure; HSC: hydrogen storage capacity; R: references.....	19
Table 2.9 MS: material structure; T: temperature; P: pressure; HSC: hydrogen storage capacity; R: references.....	20
Table 2.10 MS: material structure; AM: activation method; AC: activation condition; BET: surface area of samples; T: temperature; P: pressure; HSC: hydrogen storage capacity; R: references.....	22
Table 2.11 MS: material structure; T: temperature; P: pressure; HSC: hydrogen storage capacity; R: references.....	23
Table 2.12 MS: material structure; T: temperature; P: pressure; HSC: hydrogen storage capacity; R: references.....	24
Table 4.1 Calculated total energy (ET in Hartree), HOMO-LUMO gap (ΔE in eV), dipole moment (in Debye), binding energy per H ₂ (ΔE_b , in eV) (from DFT/B3LYP/3-21G calculations (*)) and binding energy (Eb in kcal/mol), heat of formation (HoF in kcal/mol) (from PM3 calculations (**)).....	33
Table 4.2 Calculated energies from geometry optimization using molecular mechanics method considering MM+ force field for single-wall carbon nanotubes. N _C : number of carbon atoms; R: radius in °A; L: length in °A; TE: total energy in kcal/mol.....	34
Table 4.3 Same as Table 3.2 but for different nanotubes.....	34
Table 4.4 Calculated energies from molecular dynamics with constant temperature 300K using molecular mechanics method considering MM+ force field for C(n,m) nanotubes. PE: potential energy in kcal/mol; KE: kinetic energy in kcal/mol; TE: total energy in kcal/mol; T: temperature in Kelvin.....	35

Table 4.5 B-N ring doped single-wall carbon nanotubes and calculated energies from geometry optimization using molecular mechanics method considering MM+ force field. R: radius in °A; L: length in °A; TE: total energy in kcal/mol.....	35
Table 4.6 Calculated energies from molecular dynamics with constant temperature 300K using molecular mechanics method considering MM+ force field for B-N ring doped single-wall carbon nanotubes. L: length in °A; PE: potential energy in kcal/mol; KE: kinetic energy in kcal/mol; TE: total energy in kcal/mol; T: temperature in Kelvin.....	36
Table 4.7 7H ₂ @B ₃ N ₃ C ₁₈ H ₁₂ and 14H ₂ @B ₃ N ₃ C ₁₈ H ₁₂ calculated energies from geometry optimization using molecular mechanics method considering MM+ force field. R: radius in °A; L: length in °A; TE: total energy in kcal/mol.....	49
Table 4.8 Calculated energies (in kcal/mol) from PM3, for B ₃ N ₃ C ₁₈ H ₁₂ , 6H ₂ @ B ₃ N ₃ C ₁₈ H ₁₂ , 7H ₂ @ B ₃ N ₃ C ₁₈ H ₁₂	49
Table 4.9 Calculated total energy (ET in kcal/mol), HOMO-LUMO gap (ΔE in eV), dipole moment (in Debye), binding energy per H ₂ (ΔE _b , in eV) (from DFT/B3LYP/3-21G calculations (*)) and binding energy (E _b in kcal/mol), heat of formation (HoF in kcal/mol) (from PM3 calculations (**)).....	50
Table 4.10 Calculated energies (in kcal/mol) from PM3, for 13H ₂ @B ₃ N ₃ C ₁₈ H ₁₂ , 14H ₂ @ B ₃ N ₃ C ₁₈ H ₁₂ . Binding energy per H ₂ (ΔE _b , in eV) (from PM3 calculation).....	50
Table 4.11 Calculated energies from molecular dynamics with constant temperature 300K using molecular mechanics method considering MM+ force field for C(n,m) nanotubes. PE: potential energy in kcal/mol; KE: kinetic energy in kcal/mol; TE: total energy in kcal/mol; T: temperature in Kelvin.....	54

LIST OF FIGURES

FIGURES

Figure 4.1 3D HOMO, LUMO, ESP and ED plots of C(4,4), H ₂ @C(4,4) optimized from DFT/B3LYP/3-21G results and their optimized geometries obtained from PM3 results.....	38
Figure 4.2 3D HOMO, LUMO, ESP and ED plots of CBN(4,4), 2H ₂ @CBN(4,4) optimized from DFT/B3LYP/3-21G results and their optimized geometries obtained from PM3 results.....	39
Figure 4.3 3D HOMO, LUMO, ESP and ED plots of C(7,0), CBN(7,0), 2H ₂ @CBN(7,0) optimized from DFT/B3LYP/3-21G results.....	40
Figure 4.4 C(7,0), CBN(7,0) and 2H ₂ @CBN(7,0) optimized geometries obtained from PM3 results.....	41
Figure 4.5 3D HOMO, LUMO, ESP and ED plots of CBN(4,0), C(4,0) optimized from DFT/B3LYP/3-21G results and their optimized geometries obtained from PM3 results.....	42
Figure 4.6 Hydrogen distribution inside of the carbon nonotubes having more than 9H ₂	43
Figure 4.7 Molecular dynamics averages to be taken between 0 and 1 pico second for H ₂ @CBN(7,0), H ₂ @C(7,0), and H ₂ @C(4,4) systems.....	44
Figure 4.8 Molecular dynamics averages to be taken between 0 and 1 pico second for 2H ₂ @CBN(4,2), H ₂ @C(4,2), and H ₂ @C(6,2) systems.....	45
Figure 4.9 Molecular dynamics averages to be taken between 0 and 1 pico second for 2H ₂ @C(7,5), and 3H ₂ @C(11,2) systems.....	46

Figure 4.10 3D HOMO, LUMO, ESP and ED plots of $B_3N_3C_{18}H_{12}$ and $7H_2@B_3N_3C_{18}H_{12}$ obtained from DFT/B3LYP/3-21G results and their optimized geometries obtained from PM3 results.....	51
Figure 4.11 $7H_2@B_3N_3C_{18}H_{12}$ and $14H_2@B_3N_3C_{18}H_{12}$ optimized geometries obtained from PM3 results. The distance from $B_3N_3C_{18}H_{12}$ to $7H_2$ is about 3.16Å.....	52
Figure 4.12 Molecular orbital eigenvalue spectra of the BN doped coronene model considered (DFT results). (a) HOMO: -4.928 eV; LUMO: -1.627 eV; HUMO: 80.098 eV; LOMO: -388.795 eV (b) HOMO: -4.940 eV; LUMO: -1.639 eV; HUMO: 80.849 eV; LOMO: -388.858 eV.....	53
Figure 4.13 Molecular dynamics averages to be taken between 0 and 1 pico second for $7H_2@B_3N_3C_{18}H_{12}$ and $14 H_2@B_3N_3C_{18}H_{12}$ systems.....	55

CHAPTER 1

INTRODUCTION

1.1 Introduction

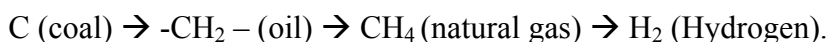
Hydrogen is the most abundant element in the universe and is found less than 1% as molecular hydrogen gas H_2 . Because of its structure, the hydrogen atom which consists of one proton and one electron is most attractive. Hydrogen has a lot of properties. First of all, it is the cleanest fuel and reduces carbon dioxide emission. The second is to have chemical energy per mass of hydrogen (39.4 kWh/kg) that is three times larger than that of other chemical fuels, such as liquid hydrocarbons (13.1 kWh/kg). In other words, the energy content of 0.33 kg of hydrogen corresponds to the energy content of 1kg of oil. The third property is its re-creating feature [1]. As a result, it can be shown the energy carrier of the future. However, it has very considerable features, we do not use it the major fuel of the world of today. Due to the fact that hydrogen is not a natural source, that is, it only can be in the form of water and hydrocarbons. Because of this, it has to be produced, which made it costing three times higher than petroleum [2]. For that reason, we want to develop any method to storage hydrogen that will be reducing the cost of hydrogen. Table 1.1 shows some important properties of hydrogen [3]. The volumetric and gravimetric density of hydrogen is important in storage material for many applications.

Table 1.1: Properties of hydrogen (data compiled from [1,2,3]).

GENERAL	
Chemical series	Nonmetals
Appearance	Colorless
Standart atomic weight	1.00794g/mol
Molecular weight	2.016 amu
Electron configuration	1s ¹
Electron per shell	1
PHYSICAL PROPERTIES	
Phase	Gas
Density	(0 °C, 101.325 kPa) 0.08988 g/L
density as liquid	70.8 kg/m ³
density as gas	36 kg/m ³
Melting point	
temperature	14.01 K (-259.14 °C)
Boiling point	
temperature	20.28 K (-252.87 °C)
Triple point	
temperature	13.8033 K
pressure	7.042 kPa
Critical point	
temperature	32.97 K
pressure	1.293MPa
density	31.40 kg/m ³
Higher heating value	141.90 MJ/kg , 11.89 MJ/m ³
Lower heating value	119.90 MJ/kg, 10.05 MJ/m ³
Heat of fusion	(H ₂) 0.117 kJ/mol
Heat of vaporization	(H ₂) 0.904 kJ/mol
Heat capacity	(25 °C) (H ₂) 28.836 J/mol.K
Self-ignition temperature	858 K
Flame temperature in air	2.318 K
Diffusion coefficient	0.61 cm ² /sn

1.2 Hydrogen Storage Methods

The improvement of energy carrier in the course of time from a solid to a gas state has been shown the series [1]:



Large amounts of hydrogen can be absorbed by many metals and alloys reversibly. Moreover, it can be stored indirectly in reactive metals such as Li, Na, Al, Zn. These metals liberate the hydrogen from the water by means of reacting with water to the corresponding hydroxide. Depending on storage size and application, several types of hydrogen storage methods are used. Due to hydrogen's low density, its storage must have large volumes, high pressures, (heavy vessels), and low temperatures [2]. Hydrogen storage fundamentals have been focused on these methods, physisorption, compression, liquefaction, chemisorption, metallic hydrides, and complex hydrides.

Before the hydrogen energy is used, there are some demands technical and economic should be carried out. The technical demands are to store hydrogen safely and conveniently. Also, to burn hydrogen efficiently is needed. The economical demand is the cost of hydrogen production. When the hydrogen is produced directly from solar light or indirectly via electricity from such renewable sources as wind-power and hydro-power, it can be a renewable fuel.

1.2.1 Physisorption

Physisorption fundamentally results from the van der Waals interaction between solids and gases. This method has been used the reversible hydrogen sorption process. Because of the interaction between the substrate (S) and the hydrogen molecule (H_2), the interaction energy appears that is calculated by the London-Dispersion forces [4]. Also, the theoretical hydrogen storage capacity (m_{ads}) is calculated from the specific surface of the carbon (S_{SPEC}) (see Table 1.2) [4].

Table 1.2: The theoretical hydrogen storage capacity formula.

The interaction energy, E_{S-H_2} (the London-Dispersion forces)
$E_{S-H_2} \propto \frac{\alpha_{H_2} \alpha_s}{R^6}$ <p>α \propto the polarizability R \propto the interaction distance</p>
The theoretical hydrogen storage capacity (m_{ads})
$m_{ads} \approx S_{spec} \times 2.27 \times 10^{-3} \text{ wt}\%$

1.2.1.1 Properties of absorbing hydrogen with physisorption

- ◆ There are two basic rules for the physisorption of supercritical gases; the monolayer adsorption mechanism and the exponential decrease of adsorption with the increasing temperature [2]. Higher temperatures will lower the adsorption capacity.
- ◆ Only a monolayer is adsorbed above the boiling point of the adsorbant [4,5].
- ◆ The adsorption capacity of hydrogen on a material depends on the specific surface area of the material [2]. Therefore, the the specific surface area of carbon nanotubes control the hydrogen uptake capacity.
- ◆ Hydrogen is desorbed with increasing temperature [4].
- ◆ Hydrogen storage capacity on graphite takes its maximum value only at very low temperature [4].
- ◆ The hydrogen adsorption increases with decreasing temperature and increasing pressure [6].
- ◆ Carbon nanotubes and high surface area graphite that reversible physisorption takes place [4].

1.3 Molecular Dynamics Simulations of H₂ Storage in Carbon Nanotubes and CBN Nanotubes

Storage of hydrogen in single wall carbon nanotubes (SWCNTs) has recently received much attention. Due to their incredible strength and electronic properties [7,8,9], these tiny carbon nanotubes have been used extensively. In this work, to obtain high hydrogen storage capacity in a stable configuration, carbon nanotubes (CNTs) [10,11] and carbon nanotubes substitutionally doped with boron nitride (CBN nanotubes) have been closely studied using various computational techniques. Hydrogen is an attractive energy source due to its high yield and the lack of environmental pollutants. Recently, five methods have been devised for storing hydrogen. These are compression, liquefaction, physisorption, metallic hydrides, and complex hydrides [12,13]. H₂ adsorption in CNTs [14] occurs by means of physisorption making it a promising method. Physisorption is based on the van der Waals interactions between adsorbed molecules and the host material, which in our case is a NT. A gas molecule interacts with several atoms on the surface of the host material during the physisorption process where it can be released reversibly. The present study has been conducted to search for ways to improve hydrogen storage in SWNTs and study how changes in the NT structure alter the storage capacity. For this aim, a boron-nitride ring has been substituted in carbon nanotubes and investigated within the density functional theory (DFT) [15]. CBN nanotubes have been studied because of their chemically stable structure. Then we can say that storage of hydrogen on undoped carbon nanotubes is less than that on CBN nanotubes. In this study, we have worked on various C(n,0) zigzag SWNTs, C(n,m) chiral SWNTs, and C(n,n) armchair SWNTs which have approximately the same length but different diameters. Also, molecular dynamics simulations (MD) have been used in order to get information about their structural properties and energetics [16]. For describing the electron properties of

atoms and molecules, we have studied PM3 semi-empirical self-consistent field molecular orbitals (SCF MO) method [17]. Moreover, to investigate the electronic structure of molecules, DFT method has been used. After that results are compared with each other.

1.4 Molecular Dynamics Simulations of H₂ Storage in BN Doped Coronene Model

Adsorption of hydrogen molecules on BN doped coronene model is investigated using the density-functional theory (DFT) method, PM3 calculation, and molecular dynamics simulations (MD). We have studied the binding energy values of H₂ molecules to 7H₂@B₃N₃C₁₈H₁₂ and 14H₂@B₃N₃C₁₈H₁₂ by means of theoretical calculations. Firstly, BN doped coronene model was prepared and was doped by means of substitution of BN. Next, different numbers of H₂ molecules were placed up position and down position of BN doped coronene model which was parallel to the hydrogen distribution. We observed that BN doped coronene model is a promising model for hydrogen storage.

CHAPTER 2

MATERIALS FOR HYDROGEN STORAGE AND THEIR CAPACITY

2.1 Introduction

Hydrogen storage values and methods of different materials have been combined with other scientific articles studied previously. There are a lot of studies about hydrogen storage which are both theoretical and experimental. This study provides an overview of experimental works on such systems to estimate the practical limits to the amount of hydrogen that could be stored per unit weight. Hydrogen storage values of carbon materials, activated carbon, graphite, carbon nanostructures, fullerene, carbon nanofibers and graphite nanofibers, carbon nanotubes and alloys have been given. Hydrogen storage methods are physisorption, chemisorption, adsorption energy, and electrochemical adsorption. Summary of the reports of gaseous hydrogen storage capacity in carbon nanotubes and carbon nanofibers, electrochemical hydrogen storage in carbon materials, the hydrogen storage behavior of alloys also have been given in the following tables.

2.2 Tables of commercial materials for hydrogen storage

Gravimetric storage of H₂ in SWNT samples was investigated near room temperature. Table 2.1a and Table 2.1b show hydrogen storage capacity of SWNTs under different conditions. All of the studies are experimental. Processing

conditions effect on the hydrogen storage capacity in these work. Therefore, different processing conditions were used. (Taken from [42])

Table 2.1a: MS: material structure; C: catalysys; PAM: purification activation method; T: temperature; P: pressure; HSC: hydrogen storage capacity; R: references.

MS	C	PAM	T (K)	P (MPa)	HSC (wt%)	R
SWNT	Co	Raw	300	0.065	0.01	[18]
SWNT	Co	Extrapolation	300	0.065	5-10	[18]
SWNT	Ni-Co	HNO ₃ /air	298	0.067	3.5-4.5	[19]
SWNT	Ni-Co-Fe-S	HCl	298	10	2.5	[20]
SWNT	Ni-Co-Fe-S	HCl/annealed	298	10	4.2	[20]
SWNT	Ni-Co	HNO ₃ /air/Ti alloy ultrasonic probe	298	0.067	6.5	[21]
SWNT	-	Ball milled	295	3.6	0.028	[22]
SWNT	-	-	295	3.6	0.05	[22]
SWNT	-	HNO ₃ /Ti alloy ultrasonic probe(1h)	298	0.08	0.04	[23]
SWNT	-	HNO ₃ / Fe alloy ultrasonic probe	298	0.08	<0.005	[23]
SWNT	Ni-Y	Raw	295	0.1	0.932	[24]
SWNT	Ni-Y	Ball milled in Ar	298	0.08	<0.1	[25]
SWNT	Ni-Y	Ball milled in D ₂	298	0.9	~1	[25]
SWNT	Ni-Co-S	Row	298	11	2.6	[26]
SWNT	Ni-Co-S	Annealed	298	11	4	[26]
SWNT	Co	HCl	295	0.9	0.02	[27]
SWNT	Co	HCl+ball milled	295	0.9	0.32	[27]
SWNT	Ni-Co	H ₂ O ₂ /HCl/NaOH	298	9	0.3	[28]
SWNT	-	Raw	300	10	<0.2	[29]
SWNT	-	Raw	298	7	0.14	[30]

Table 2.1b: MS: material structure; C: catalysts; PAM: purification activation method; T: temperature; P: pressure; HSC: hydrogen storage capacity; R: references.

MS	C	PAM	T (K)	P (Mpa)	HSC (wt%)	R
SWNT		Raw	298	7	0.43	[30]
SWNT	Ni-Y	Raw	295	10	2.9	[31]
SWNT	-	Raw	298	4.8	0.29	[32]
SWNT	-	HNO ₃ /CO ₂ /annealed	298	4.8	1.2	[32]
SWNT	Mo-Co	Raw	298	12	0.45	[33]
SWNT	Ni-Y	Air	300	14	0.2	[34]
SWNT	Ni-Y	Air/HNO ₃	300	14	0.4	[34]
SWNT	Ni-Co	Toluene/air/HCl	298	3	0.4	[35]
SWNT	-	-	294	30	0.91	[36]
SWNT	-	Raw	303	3.1	0.12	[37]
SWNT	-	HNO ₃	303	3.1	0.25	[37]
SWNT	-	Raw	295	0.1	0.06	[38]
SWNT	-	-	295	0.1	0.1-0.2	[38]
SWNT	Ni-Y	KOH	298	0.1	0.02	[39]
SWNT	Fe-Co	Raw	298	4	0.07	[40]
SWNT	Fe-Co	HCl	298	4	0.63	[40]
SWNT	Ni-Co	Raw	253	6	0.4-1	[41]

Gaseous hydrogen storage capacity were investigated in both SWNTs and MWNTs. Table 2.2a and Table 2.2b show hydrogen storage values between 0.05 and 21 wt%. However, the high values have not been verified. We can say that the storage values are dependent on many parameters of the carbon nanotubes, such as structure, structure defects, geometry, storage pressure, temperature. All of the studies are experimental in Table 2.2a and Table 2.2b. (Taken from [69])

Table 2.2a: MS: material structure; C: catalysts; PAM: purification activation method; T: temperature; P: pressure; HSC: hydrogen storage capacity; R: references.

MS	P (%)	T (K)	P (MPa)	HSC (wt%)	R
SWNT	Assumed 100	133	0.04	5-10	[43]
SWNT	High	Ambient	0.067	3.5-4.5	[44]
SWNT	~50	300	10.1	4.2	[45]
Aligned SWNT	Purified	Ambient	11	4	[46]
SWNT	Purified	77-300	8	1-15	[47]
SWNT	High	80	~7	8.25	[48]
MWNT	Purified	~300-700	Ambient	0.25	[49]
SWNT	Purified	Ambient	4.8	1.2	[50]
SWNT-TiAl _{0.1} V _{0.04}	Sonicated >98	Ambient	0.067	6	[51]
SWNT-Ti-6Al-4V	Purified	Ambient	0.08	1.7	[52]
SWNT-Fe	Purified	Ambient	0.08	<0.005	[52]
Ball-milled SWNT in Ar	<50	Ambient	0.08	<0.1	[53]
Ball-milled SWNT in D ₂	<50	Ambient	0.9	0	[53]
CNT	Purified	298-773	0.1	0	[53]
Doped CNT	-	-	-	0.5-1.0	[54]
Li-CNT	Purified	473-673	0.1	20	[55]
K-CNT	Purified	<313	0.1	14	[55]
Li-CNT (wet H ₂)	Purified	473-673	0.1	12	[56]
Li-CNT (dry H ₂)	Purified	473-673	0.1	2.5	[56]
K-CNT (wet H ₂)	Purified	<313	0.1	21	[56]
K-CNT (dry H ₂)	Purified	<313	0.1	1.8	[56]
Li-CNT	10-40	473-663	0.1	0.7-4.2	[57]
SWNT	80-90	273	0.04	7	[51]

Table 2.2b: MS: material structure; C: catalysts; PAM: purification activation method; T: temperature; P: pressure; HSC: hydrogen storage capacity; R: references.

MS	P (%)	T (K)	P (MPa)	HSC (wt%)	R
SWNT	90 vol%	298	-	0.63	[58]
MWNT	Unpurified	298	-	0.5	[59]
MWNT	Unpurified	293	6.5	2	[59]
CNT	-	Ambient	Ambient	0.5	[60]
SWNT	Purified	77	0.2	6	[61]
Aligned MWNT	High	298	10	3	[62]
Aligned MWNT	High	290	10	2.4	[63]
Random MWNT	High	298	10	0.68	[62]
MWNT	High untreated	300	1.0	5-7	[64]
MWNT	High acid treated	300	1.0	13.8	[64]
MWNT	High	300	7.0	0.7-0.8	[65]
SWNT	Unpurified	295	0.1	0.93	[66]
SWNT	Unpurified	77	0.1	2.37	[67]
MER MWNT	10-15%	298	3.6	0.03	[67]
Rice SWNT	High	298	3.6	0.05	[67]
CNT	-	298	11.35	11.26	[68]

Hydrogen gas storage capacity are investigated in carbon nanofibers. Table 2.3 shows values of H₂ storage under different conditions in carbon nanofibers. Hydrogen storage values are between 0.1 and 67.55 wt%. 67.55wt% and 53.68 wt% values are extraordinary. None of these high values has been reproduced in other laboratories. Both the synthesis and purification conditions and the pretreatment of the grafit nanofibers influence the storage hydrogen capacities.

(Taken from [69])

Table 2.3: MS: material structure; C: catalysts; PAM: purification activation method; T: temperature; P: pressure; HSC: hydrogen storage capacity; R: references.

MS	P (%)	T (K)	P (MPa)	HSC (wt%)	R
GNF herringbone	-	298	11.35	67.55	[68]
GNF platelet	-	298	11.35	53.68	[68]
GNF	-	77-300	0.8-1.8	0.08	[70]
CNF	-	300	12	6.5	[71]
GNF	-	300	10.5	0.7	[72]
CNF	-	293	10	1	[73]
CNF	-	298	12	1.4	[74]
Ball milled GNF	-	Ambient	0.9	0.5	[53]
GNF	-	300	11	<0.1	[75]
Vapor grown carbon fibers	-	298	3.6	<0.1	[67]
CNF	-	300	12.5	1.6	[76]
GNF Herringbone	Purified	77-300	1.5	1-1.8	[76]
GNF	-	300	12	10	[77]
GNF	-	300	12	10	[78]
CNF	-	77	12	12.38	[79]
CNF	-	300	11	5.7	[80]

Electrochemical hydrogen storage was investigated in carbon materials. Table 2.4 shows the hydrogen storage capacity between 0.27wt% and 2.9wt% , with the exception of the 6.1wt% value of Liu. 6.1wt% has not been reproduced by other groups. Gold, nickel, copper, or palladium are used as the form of micrometer-sized powders or nanosized particles that were used for decorating the carbon surface like additives. The storage capacity is increased in the presence of metals. The catalyst, the electrolyte, the carbon material, the charge and discharge conditions, and the atmosphere influence the storage capacity. (Taken from [69])

Table 2.4: MS: material structure; EC: experimental conditions; T: temperature; P: pressure; HSC: hydrogen storage capacity; R: references.

MS	EC	T (K)	P (atm)	HSC (wt%)	R
SWNT-Pd powder(1:4)	6M KOH $I_{\text{disch}}=2.5-5\text{Ag}^{-1}$	Room temperature	1	0.39	[81]
Activated carbon(1200-1500 m^2g^{-1})	6M KOH $I_{\text{disch}}=100\text{mA}\text{g}^{-1}$	Room temperature	1	1.5	[82]
MWNT/Ni(1:10)	6M KOH $I_{\text{disch}}=200-1000\text{mA}\text{g}^{-1}$	Room temperature	1	0.7	[83]
CNT/Ni powder(4:5)	6M KOH $I_{\text{disch}}=0.4\text{mA}\text{g}^{-1}$	Room temperature	1	0.34	[84]
SWNT/Cu (1:3)	30% KOH $I_{\text{disch}}=10-100\text{mA}\text{g}^{-1}$	Room temperature	1	2.9	[85]
HNO ₃ treated CNF/Ni	6M KOH $I_{\text{disch}}=100\text{mA}\text{g}^{-1}$	Room temperature	1	0.27	[86]
SWNT/Ni powder(1:3)	6M KOH $I_{\text{disch}}=400\text{mA}\text{g}^{-1}$	Room temperature	1	1.2	[87]
CNF/Ni-P particles+Ni powder(1:3)	6N KOH $I_{\text{disch}}=1000\text{mA}\text{g}^{-1}$	Room temperature	1	1.1	[88]
CNF/Ni-P particles(<76)	6M KOH $I_{\text{disch}}=1000\text{mA}\text{g}^{-1}$	Room temperature	1	0.30	[89]
MWNT (electrochem.)	18M H ₂ SO ₄ 20 °C Cyclic voltammetry	Room temperature	1	1.61	[90]
CNT/Ni powder (1:20)	6N KOH $I_{\text{disch}}=800\text{mA}\text{g}^{-1}$	Room temperature	1	1.0,0.25	[91]
MWNT/Cu particles	6M KOH $I_{\text{disch}}=1500\text{mA}\text{g}^{-1}$	Room temperature	1	6.1	[92]
SWNT pressed into Ni foam	6M KOH $I_{\text{disch}}=25\text{mA}\text{g}^{-1}$	Room temperature	1	1.84	[93]
Electrochem. Ox. MWNT in HNO ₃	6M KOH and 0.3M H ₂ SO ₄ CV and $I_{\text{disch}}=20\text{mA}\text{g}^{-1}$	Room temperature	1	0.3	[94]

Microstructure of Mg_3La and $\text{Mg}_3\text{LaNi}_{0.1}$ alloys were studied for their hydrogen storage capacity under different conditions. X-ray diffraction and pressure–composition isotherm measurement were used to investigate alloys. The Mg_3La and $\text{Mg}_3\text{LaNi}_{0.1}$ alloys both exhibit rapid hydriding and dehydriding kinetics. Mg-based alloys are considered to offer significant potential on account of their high hydrogen storage capacity and their abundance.

Nanocrystalline Mg- x wt.% Cr_2O_3 ($x = 5\text{--}20$) composites were prepared by ball milling Mg and nanocrystalline Cr_2O_3 under toluene. Table 2.5 shows the absorption and desorption capacities of these composites. The absorption capacities decreased with decrease in temperature in each of the compositions. All of the studies in Table 2.5 are experimental.

Table 2.5: MS: material structure; T: temperature; P: pressure; HSC: hydrogen storage capacity; R: references.

MS	T (°C)	P (Mpa)	HSC (wt%)		R
Mg ₃ La (Alloy)	297	(Max) 3.8	2.89		[95]
Mg ₃ LaNi _{0.1} (Alloy)	257	(Max) 3.8	2.73		[95]
Mg-5 wt.% Cr ₂ O ₃ (nanocomposite)	T (°C)	Desorption Pressure (bar)	Absorption Capacity (wt.%)	Desorption Capacity (wt.%)	
	300	1.36	6.01	3.19	[96]
	200	0.40	5.67	0.57	
	100	0.10	0.31	0.01	
Mg-10 wt.% Cr ₂ O ₃ (nanocomposite)	300	1.56	5.54	3.66	[96]
	200	0.50	4.91	0.76	
	100	0.10	0.91	0.01	
Mg-15 wt.% Cr ₂ O ₃ (nanocomposite)	300	1.85	5.45	4.02	[96]
	200	0.49	5.30	0.64	
	100	0.51	3.80	0.64	
Mg-20 wt.% Cr ₂ O ₃ (nanocomposite)	300	1.61	4.94	3.77	[96]
	200	0.63	4.61	1.02	
	100	0.52	3.27	0.69	

Chemically activated carbons with a wide range of porosities were studied to investigate their hydrogen storage capacity under different temperatures (298 K and 77 K) and high pressure. Both the micropore volume and the micropore size distribution affect the hydrogen adsorption capacity at 298 K. The surface area and the total micropore volume of the activated carbon affect hydrogen adsorption at 77 K. Super activated carbons; samples of the series KUA which has surface areas higher than 3000 m²/g. All of the studies in Table 2.6 are experimental. Table 2.6 shows that highly activated carbons have a great potential as carriers of hydrogen.

Table 2.6: MS: material structure; T: temperature; P: pressure; HSC: hydrogen storage capacity; KUA5: A chemically activated carbon; KUA6: Activated carbon R: references.

MS	T (K)	P (Mpa)	HSC (wt%)	R
KUA5	298	20	1.2	[97]
KUA5	298	50	2.7	
KUA5	77	4	5.6	
KUA5	298	20	3.2	
KUA5	298	50	6.8	
KUA6	77	4	8.0	
KUA5	77	4	7.1	

Reactive ball milling (RBM) of a mixture of Mg and Ti_{1.0}V_{1.1}Mn_{0.9} alloy powders was used to obtain Mg-30 wt.% Ti_{1.0}V_{1.1}Mn_{0.9} composites. The catalyst

was $Ti_{1.0}V_{1.1}Mn_{0.9}$ to improve the hydriding/dehydriding properties of Mg in this study. Mg was considered the main hydrogen absorbing material in this work.

S-1, S-2, and S-3 were different samples under different preparation conditions of the Mg-30 wt.% $Ti_{1.0}V_{1.1}Mn_{0.9}$ composites. The sample S-3 had the best hydrogen absorption/desorption kinetics and largest hydrogen storage capacity among the three samples. All of the studies are experimental in Table 2.7.

Table 2.7: MS: material structure; T: temperature; P: pressure; S: samples ; R: references.

MS	S	T (K)	P (MPa)	Hydrogen absorption capacity (wt%)	Hydrogen desorption capacity (wt%)	R
Mg-30 wt.% $Ti_{1.0}V_{1.1}Mn_{0.9}$	S-1	606	0.2	2.73	2.73	[98]
		573	0.2	2.29	2.29	
		528	0.2	2.01	0.10	
		483	0.2	1.16	0.07	
		377	0.2	0.43	0.10	
	S-2	606	0.4	3.41	3.24	
		573	0.4	3.03	1.59	
		528	0.4	2.56	0.08	
		483	0.4	1.76	0.06	
		377	0.4	0.62	0.09	
	S-3	606	0.4	4.46	4.32	
		573	0.4	4.44	4.23	
		528	0.4	4.33	0.25	
		483	0.4	3.99	0.06	
		377	0.4	1.77	0.08	

Reactive mechanical alloying (RMA) was used to prepare Mg–20 wt% Ni–Y composite. The hydrogen storage capacity of Mg–20 wt% Ni–Y composite is higher than 5.2 wt% under different temperatures. Mg–20 wt% Ni–Y composite exhibits a high hydrogen storage capacity and excellent hydrogen sorption kinetics. All of the studies are experimental in Table 2.8.

Table 2.8: MS: material structure; T: temperature; P: pressure; HSC: hydrogen storage capacity; R: references.

MS	T (K)	P (MPa)		HSC (wt%)		R
		Absorption Pressure (MPa)	Desorption Pressure (MPa)	Absorption Capacity (wt.%)	Desorption Capacity (wt.%)	
Mg– 20 wt% Ni–Y (nanocomposite) Purity (%) Mg >99.8 Ni >99.9 Y >99.5						[99]
	293	3.0		4.16		
	473	3.0		5.59		
	573		0.1		4.75	

Mechanical milling Mg–Ce hydrides and nano-sized Ni powder was used to prepare Mg–Ce/Ni composite. The addition of Ni and Ce improve the activation properties of Mg-based hydrogen storage material. Mg–Ce/Ni composite showed

significant hydriding/dehydriding performance. All of the studies in this work are experimental in Table 2.9.

Table 2.9: MS: material structure; T: temperature; P: pressure; HSC: hydrogen storage capacity; R: references.

MS	S	T (K)	P (MPa)	HSC (wt%)	REF.
Nanocrystalline Mg-Ce/Ni composite (Mg-10.9wt.%Ce/ 10.0 wt.% Ni)	Pure Mg	At different temperatures	Absorption Pressure (MPa)	Absorption Capacity (wt.%)	[100]
		393	4	0.57	
		413	4	2.85	
		433	4	3.76	
		453	4	4.40	
		473	4	5.39	
	Mg/ 10.0 wt.% Ni	393	4	2.16	
		413	4	2.88	
		433	4	3.18	
		453	4	4.12	
		473	4	5.33	
	Mg- 10.9 wt.% Ce/ 10.0 wt.% Ni	393	4	2.92	
		413	4	4.05	
		433	4	4.94	
		453	4	5.30	
		473	4	-	
			Desorption Pressure (MPa)	Desorption Capacity (wt.%)	
		453	0.1	2.12	

Physical activation with CO₂ and chemical activation with KOH were used as activation systems in this study. Table 2.10 shows that to increase hydrogen storage capacity, an increase in BET surface area does not work some of the systems. All of the studies are experimental in Table 2.10.

The mechanical alloying process was used to obtain nanostructured composite materials Mg–Ni, Mg–Ni–La, Mg–Ni–Ce and Mg–LaNi₅. The purity and particle size are 99.5% and 100µm. All of the studies are experimental in Table 2.11.

Hydriding combustion synthesis was used to prepare Mg_{1.95}Ag_{0.05}Ni, Mg_{1.9}Ag_{0.1}Ni, Mg_{1.5}Ag_{0.5}Ni investigated by pressure–composition isotherms, X-ray diffraction and scanning electron microscopy. All of the studies are experimental in Table 2.12.

Table 2.10: MS: material structure; AM: activation method; AC: activation condition; BET: surface area of samples; T: temperature; P: pressure; HSC: hydrogen storage capacity; R: references.

MS	AM	AC	BET (m ² g ⁻¹)	T (°C)	P (MPa)	HSC (wt%)	R
Carbon Nanofibers from Cu ₂₀ Ni ₈₀ (Cu ₂₀ Ni ₈₀ CNF)	Activated by CO ₂ (Physical activation)	As prepared	475	30	10	0.35	101
		900 °C 15 min	472	30	10	-	
		900 °C 30 min	465	30	10	0.26	
		900 °C 45 min	458	30	10	0.22	
		800 °C 30 min	476	30	10	0.28	
		800 °C 120 min	488	30	10	-	
		825 °C 30 min	478	30	10	0.31	
		825 °C 120 min	517	30	10	0.30	
		825 °C 480 min	678	30	10	-	
		850 °C 30 min	482	30	10	0.33	
		850 °C 120 min	521	30	10	-	
		875 °C 30 min	477	30	10	0.27	
	875 °C 120 min	542	30	10	-		
	Activated by KOH (Chemical activation)	As prepared	475	30	10	0.35	
		900 °C 30 min	1000	30	10	0.42	
		900 °C 60 min	725	30	10	0.34	
		900 °C 90 min	674	30	10	-	
		900 °C 120 min	689	30	10	-	
Carbon Nanofibers from Fe ₂₀ Ni ₈ (Fe ₂₀ Ni ₈ CNF)	Activated by CO ₂ (Physical activation)	As prepared	150	30	10	0.07	101
		900 °C 15 min	171	30	10	-	
		900 °C 30 min	194	30	10	0.05	
		900 °C 45 min	169	30	10	<0.04	
		1000 °C 15min	143	30	10	-	
		1000 °C 15min	158	30	10	0.06	
	Activated by KOH (Chemical activation)	As prepared	150	30	10	0.07	
		500 °C 30 min	144	30	10	-	
		700 °C 30 min	227	30	10	<0.04	
		900 °C 30 min	230	30	10	0.05	

Table 2.11: MS: material structure; T: temperature; P: pressure; HSC: hydrogen storage capacity; R: references.

MS	T (°C)	HSC (wt%)		REF.
		Absorption capacity (wt%) at 3MPa	Desorption capacity (wt%) at vacuum	
Mg 70 wt.%– Ni 20 wt.%– La 10 wt.%	25	1.8	1.0	[102]
	100	1.9	1.0	
	200	4.0	1.0	
	300	5.4	4.5	
Mg 60 wt.%– Ni 30 wt.%– La 10 wt.%	25	1.0	0.7	
	100	1.7	1.0	
	200	2.1	3.0	
	300	5.2	4.6	
Mg 80 wt.%– LaNi ₅ 20 wt.%	25	1.9	1.7	
	100	2.4	1.9	
	200	2.9	2.3	
	300	5.5	4.2	
Mg 75 wt.%– LaNi ₅ 25 wt.%	25	0.6	0.4	
	100	0.7	0.7	
	200	1.7	0.7	
	300	4.9	4.5	
Mg 60 wt.%– LaNi ₅ 40 wt.%	25	1.1	0.3	
	100	1.1	0.4	
	200	1.3	0.5	
	300	3.6	3.3	

Table 2.12: MS: material structure; T: temperature; P: pressure; HSC: hydrogen storage capacity; R: references.

MS	T (K)	P (MPa)		HSC (wt%)		R
		Absorption Pressure (MPa)	Desorption Pressure (MPa)	Absorption Capacity (wt.%)	Desorption Capacity (wt.%)	
Mg _{1.95} Ag _{0.05} Ni	573	1	0.1	3.62	3.47	103
	553	1	0.1	3.49	3.31	
	523	1	0.1	3.47	3.30	
Mg _{1.9} Ag _{0.1} Ni	573	1	0.1	3.48	3.36	
	553	1	0.1	3.43	3.18	
	523	1	0.1	3.28	3.16	
Mg _{1.5} Ag _{0.5} Ni	573	1	0.1	2.31	-	
	553	1	0.1	-	1.87	
	523	1	0.1	1.97	-	

CHAPTER 3

METHOD OF CALCULATION

3.1.1 Computational Methods

Molecular mechanics method has been used to obtain the stable configurations of the molecules that minimizes the interaction energies between the atoms of a system. One of the optimization method is a conjugate gradient method (the Polak-Ribiere algorithm) used in this study that finds the local minimum of the systems.

To describe the electron properties of atoms and molecules, the semi-empirical methods have been used that solve the Schrödinger equation, with certain approximations. The electronic Schrödinger equation is:

$$\hat{H}_e \Psi_e = (\hat{H}_{k,e} + \hat{H}_{p,e-e} + \hat{H}_{p,n-e}) \Psi_e = E_e \Psi_e$$

where k,p,n,e show by turns the kinetic energy, the potential energy, the nucleus and the electrons. Parametric method number 3 (PM3) used in the study is one of the semi-empirical methods.

The main idea of density functional theory (DFT) is that instead of solving the Schrödinger equation for the wavefunction describes an interacting system of any particle via its density $\rho(\vec{r})$. From DFT calculations, total energy (ET in Hartree), HOMO-LUMO gap (ΔE in eV), dipole moment (in Debye) was obtained in the study.

Molecular Dynamics used in the study simulates molecular movement that provides to find equilibrium properties and kinetic behavior of molecules.

3.1.2 DFT Studies for Carbon Nanotubes and CBN Nanotubes

Many theoretical studies have been performed recently to predict the hydrogen storage capacity of carbon nanostructures by means of theoretical calculations. In the present work, we have studied various structures of carbon nanotubes, and CBN nanotubes. Firstly, CNTs were prepared and some were doped by means of substitution of a BN ring. Next, different numbers of H₂ molecules were placed inside the bare carbon nanotube and the substitutionally doped carbon nanotube structures to compare the electronic properties. The systems under study were obtained from the geometries of C(4,4), C(4,0), C(7,0), H₂@C(4,4), and substitutionally BN doped structures CBN(4,4), H₂@CBN(4,4), 2H₂@CBN(4,4), CBN(7,0), H₂@CBN(7,0), 2H₂@CBN(7,0), CBN(4,0). In all of these calculations carbon atoms at the ends of the tubes were saturated by hydrogen atoms to remove the dangling bonds and make the coordination number of all the carbon atoms the same.

The structures of the models were optimized by applying the molecular-mechanics (MM) method using MM+ force field [104], which makes easier to perform full optimization by extended methods. The semi-empirical self-consistent-field molecular orbital (SCF-MO) method at PM3 level within the restricted Hartree-Fock (RHF) formalism [104] has been applied to optimize fully the geometry of the models considered. These calculations have been carried out

with HyperChem 7.5 program package [105]. Also, Polak-Ribiere optimizer [106] was used in geometry optimizations. The SCF convergence criterion was taken to be 0.001 kcal /A.mol. Single point electronic calculations were performed using DFT with the B3LYP exchange-correlation functional [107,108] in the 3-21G basis set [109]. We used both HyperChem 7.5 package and Gaussian 03 package [110] for DFT calculations. We calculated total energy, HOMO-LUMO gap, dipole moment, binding energy, and heat of formation for the systems studied. More details about DFT with the B3LYP can be found in Ref. [111, 112, 113].

3.1.3 Molecular Mechanics Method Studies for Carbon Nanotubes and CBN Nanotubes

In this work, the hydrogen distribution inside the carbon nanotubes having more than 9H₂ has been predicted by molecular mechanics method. For comparing results to be taken different carbon nanotubes, we have studied C(n,0) zigzag SWNTs, C(n,m) chiral SWNTs, and C(n,n) armchair SWNTs having approximately the same length and the same radius. First, four carbon nanotubes were prepared in vacuum. Next, all four models, 14H₂@C(7,7), 20H₂@C(8,8), 16H₂@C(14,0), and 10H₂@C(11,2), were geometry optimized using molecular mechanics method considering the MM+ force field. Similarly CBN nanotubes were investigated. When the number of H₂ molecules placed inside exceeded 9, the CBN(4,4) and CBN(7,0) were observed to break using molecular mechanics method considering MM+ force field.

3.1.4 Molecular Dynamics Simulation Studies for Carbon Nanotubes and CBN Nanotubes

$H_2@CBN(7,0)$, $H_2@C(7,0)$, $H_2@CBN(4,4)$, $2H_2@C(4,2)$, $H_2@C(4,2)$, $H_2@C(6,2)$, $2H_2@C(7,5)$, $3H_2@C(11,2)$ were prepared. We calculated energies from molecular dynamics at a constant temperature of 300K using molecular mechanics method with MM+ force field. Molecular dynamics averages were taken between 0 and 1 picosecond. Results are presented as a graph in section 4.1.3.

3.2.1 DFT Studies for BN Doped Coronene Model

The structure of the BN doped coronene model was optimized by applying the molecular mechanics (MM) method using MM+ force field. The semi-empirical self-consistent field molecular orbital (SCF-MO) method at PM3 level within the restricted Hartree-Fock (RHF) formalism has been applied to optimize fully the geometry of the models considered. Polak-Ribiere optimizer was used in geometry optimizations. The SCF convergence limit was set to 0.001 kcal/mol to get sufficient structural optimization. Single point electronic calculations were performed using density functional theory (DFT) considering B3-LYP exchange-correlation functional in 3-21G basis set. We investigated the binding energy of H_2 molecules to $B_3N_3C_{18}H_{12}$ and calculated HOMO-LUMO gap, dipole moment, and heat of formation for $7H_2@B_3N_3C_{18}H_{12}$. To investigate total energy and the binding energy of H_2 molecules to $14H_2@B_3N_3C_{18}H_{12}$, we used PM3 calculation.

3.2.2 Molecular Dynamics Simulation Studies for BN Doped Coronene Model

We have investigated MD simulation at room temperature to test the stability of $7\text{H}_2@ \text{B}_3\text{N}_3\text{C}_{18}\text{H}_{12}$ and $14 \text{H}_2@ \text{B}_3\text{N}_3\text{C}_{18}\text{H}_{12}$ using molecular mechanics method with MM+ force field. Run time were taken 1 picosecond (ps) and step size were taken 1×10^{-3} ps at constant temperature of 300K. Results are presented graphically in section 4.2.2.

CHAPTER 4

RESULTS AND DISCUSSION

4.1.1 DFT Study Results for Carbon Nanotubes and CBN Nanotubes

Using DFT calculations, we calculated the binding energy of stored hydrogen. The binding energy of H₂ molecules in CBN nanotubes is greater than that of undoped nanotubes. In addition to this, a stable system is defined to have a negative binding energy in this study. The binding energy calculated per H₂ molecule for H₂@C(4,4) (in Hartree) is defined as follows :

$$\Delta E_{bind} = E(H_2@C(4,4)) - E(H_2) - E(C(4,4)) \quad (1)$$

where $E(H_2@C(4,4))$, $E(C(4,4))$, and $E(H_2)$ are the total energies of fully optimized H₂@C(4,4) structure, the nanotube alone, the hydrogen molecule, respectively. From this calculation, a positive binding energy was obtained. For this reason, H₂@C(4,4) is not a stable system. To obtain a stable system, a boron-nitride ring was substituted in carbon nanotubes.

From DFT calculations that gives total energy value for systems, it can be observed that a boron-nitride ring increases storage capacity in CNT. In the same way, the binding energy per H₂ molecule for 2H₂@C(4,4) substitutionally doped

with BN was calculated as follows:

$$\Delta E_{bind} = E(H_2@CBN(4,4)) - E(H_2) - E(CBN(4,4)) \quad (2)$$

The total energies taken from Table 4.1, $E(H_2)$, $E(CBN(4,4))$, $E(H_2@CBN(4,4))$, show that E_{bind} per H_2 molecule for $2H_2@CBN(4,4)$ is -0.27 eV. Therefore, we conclude that $2H_2@CBN(4,4)$ is a stable system. Table 4.2 and Table 4.3 gives information about total energies of the molecules under study. $H_2@C(4,4)$ and $H_2@CBN(4,4)$ have the same length and the same radius, which is shown in Table 4.4-4.6.

Before calculating the total energy, we placed one H_2 molecule inside the CBN(4,4). After putting each H_2 molecule, we calculated total energy of the system. This procedure was continued in the same way until the CBN(4,4) was not able to store any additional H_2 molecule in it (using molecular mechanics method considering MM+ force field); in other words, a CBN(4,4) was not able to store 3 H_2 molecules in it. Finally, E_{bind} per H_2 molecule for $2H_2@CBN(7,0)$ was obtained the same way that shows $2H_2@C(7,0)$ is a stable system. We make an additional observation that E_{bind} per H_2 molecule for $2H_2@CBN(7,0)$ is larger than E_{bind} per H_2 molecule for $2H_2@CBN(4,4)$. We thus conclude that a boron-nitride ring in the CBN nanotubes enhances the hydrogen storage capacity.

3D plots of the highest occupied molecular orbital (HOMO) and the lowest unoccupied molecular orbital (LUMO), electrostatic potential (ESP), and electron density (ELDEN) figures, and optimized geometries obtained from PM3 results of the systems studied are shown in Figure 4.1-4.5, respectively. ELDEN plots for all molecules show a uniform distribution. From ESP figures, positive ESP plots for all molecules except for CBN(4,0) show a homogeneous distribution. In addition to this, while negative ESP is found to be in the vicinity of the boron-nitride ring for CBN(4,0), positive ESP is found over the rest of the molecules.

HOMO and LUMO can give some information about chemical reactivity and kinetic stability of the CNTs and CBN nanotubes. The systems with a small HOMO-LUMO gap has a high chemical reactivity and low kinetic stability [114]. It can be seen from Table 4.1 that C(7,0) is chemically more reactive than others. On the other hand, CBN(4,4) is more stable than the others. CBN nanotubes have a greater HOMO-LUMO gap compared to undoped CNTs. While the HOMO and LUMO plots for C(4,4), and H₂@C(4,4) display a uniform distribution, the HOMO and LUMO plots for CBN nanotubes are found to be in a certain region.

Formation of all the models are endothermic except CBN(7,0), H₂@CBN(7,0), 2H₂@CBN(7,0) which are exothermic. Table 4.1 shows the calculated dipole moment values. The CNT and CBN nanotubes have dipole moments due to non-uniform distribution of charges on the various atoms. CBN(7,0), H₂@CBN(7,0), 2H₂@CBN(7,0), and CBN(4,4) have dipole moments that greater than the rest of the NTs considered. When the molecules become greater dipole moment, intermolecular forces such as boiling point, melting point, become stronger. This gives us information about stability of the structures that has been used for molecular dynamics simulation in this work.

Table 4.1: Calculated total energy (ET in Hartree), HOMO-LUMO gap (ΔE in eV), dipole moment (in Debye), binding energy per H₂ (ΔE_b , in eV) (from DFT/B3LYP/3-21G calculations (*)) and binding energy (E_b in kcal/mol), heat of formation (HoF in kcal/mol) (from PM3 calculations (**)).

System	ET(*)	ΔE (*)	μ (*)	ΔE_b (*)	E_b (**)	HoF(**)
H ₂	-1.17	0.31	0.00	–	-116.00	-11.80
C(4,4)	-2416.70	1.60	0.04	–	-11139.00	631.58
H ₂ @C(4,4)	-2417.78	1.58	0.01	2.44	-11224.47	650.33
CBN(4,4)	-2476.44	2.50	0.58	–	-10429.53	224.09
H ₂ @CBN(4,4)	-2477.62	2.50	0.56	-0.27	-10537.61	220.22
2H ₂ @CBN(4,4)	-2478.80	2.50	0.74	–	-10643.41	218.63
C(7,0)	-2130.22	0.52	0.00	–	-9606.97	692.30
CBN(7,0)	-2179.02	1.88	4.61	–	-9096.31	-100.15
H ₂ @CBN(7,0)	-2180.21	1.88	4.54	–	-9203.01	-102.65
2H ₂ @CBN(7,0)	-2181.40	1.88	4.59	-0.54	-9309.40	-104.84
C(4,0)	-1216.78	2.21	0.05	–	-5033.40	851.89
CBN(4,4)	-1244.60	1.14	3.03	–	-4810.04	330.61

Table 4.2: Calculated energies from geometry optimization using molecular mechanics method considering MM+ force field for single-wall carbon nanotubes. N_C : number of carbon atoms; R: radius in °A; L: length in °A; TE: total energy in kcal/mol.

Quantity	N_C	R	L	TE
14H ₂ @C(7,7)	168	4.75	12.30	683.93
20H ₂ @C(8,8)	192	5.43	12.30	667.37
16H ₂ @C(14,0)	196	5.48	12.78	- 81.55
10H ₂ @C(11,2)	196	4.75	14.41	842.20

Table 4.3: Same as Table 2 but for different nanotubes.

Quantity	N_C	R	L	TE
2H ₂ @C(7,5)	134	4.09	12.30	670.13
H ₂ @C(6,2)	104	2.82	13.01	849.13
3H ₂ @C(11,2)	196	4.75	14.41	842.20

Table 4.4: Calculated energies from molecular dynamics with constant temperature 300K using molecular mechanics method considering MM+ force field for C(n,m) nanotubes. PE: potential energy in kcal/mol; KE: kinetic energy in kcal/mol; TE: total energy in kcal/mol; T: temperature in Kelvin.

Quantity	PE	KE	TE	T
2H ₂ @C(7,5)	816.64	152.33	968.97	311.61
H ₂ @C(6,2)	957.86	121.07	1078.93	322.36
3H ₂ @C(11,2)	1082.43	210.73	1293.16	302.12

Table 4.5: B-N ring doped single-wall carbon nanotubes and calculated energies from geometry optimization using molecular mechanics method considering MM+ force field. R: radius in °A; L: length in °A; TE: total energy in kcal/mol.

Quantity	# atoms	R	L	TE
2H ₂ @CBN(7,0)	14B,14N,28C	2.74	7.10	272.37
H ₂ @C(7,0)	56C	2.74	7.10	471.71
2H ₂ @CBN(4,4)	12B,12N,40C	2.71	8.64	385.27
H ₂ @C(4,4)	64C	2.71	8.64	550.76
2H ₂ @CBN(4,2)	10B,9N,37C	2.07	9.94	531.61
H ₂ @C(4,2)	56C	2.08	9.94	733.17

Table 4.6: Calculated energies from molecular dynamics with constant temperature 300K using molecular mechanics method considering MM+ force field for B-N ring doped single-wall carbon nanotubes. L: length in °A; PE: potential energy in kcal/mol; KE: kinetic energy in kcal/mol; TE: total energy in kcal/mol; T: temperature in Kelvin.

Quantity	L	PE	KE	TE	T
H ₂ @CBN(7,0)	7.10	345.24	59.85	405.09	278.86
H ₂ @C(7,0)	7.10	555.87	45.90	601.78	213.89
H ₂ @CBN(4,4)	8.64	453.02	76.50	529.48	312.81
2H ₂ @CBN(4,2)	9.94	600.72	73.50	674.21	324.39
H ₂ @C(4,2)	9.94	803.66	65.62	869.28	297.48

4.1.2 Molecular Mechanics Method Study Results for Carbon Nanotubes and CBN Nanoubes

When the CNT has a radius larger than 4.7 °A, the H₂ molecules distribute on a helix-like path using molecular mechanics method considering MM+ force field.

Table 4.2 lists the dependence of H₂ distribution on system parameters of the NTs studied. In addition to this, as seen from Figure 4.6, H₂ molecules do not distribute uniformly in a tube with a radius larger than 4.7 °A, although they keep helix-like path formation.

4.1.3 Molecular Dynamics Simulation Study Results for Carbon Nanotubes and CBN Nanotubes

Tables 4.3–4.6 display the total energies of several nanotubes with varying length and radius. Table 4.3 shows total energy values for $2\text{H}_2@\text{C}(7,5)$, $\text{H}_2@\text{C}(6,2)$, and $3\text{H}_2@\text{C}(11,2)$. It has been found that the radius and the length of CNTs and number of carbon atoms in CNTs affect total energy values of the CNTs. From the data of Tables 4.5 and 4.6 we can deduce the following: In static calculations (MM/MM+) it was found that the NTs CBN(7,0) and CBN(4,4) can store 2H_2 molecules. However, in molecular dynamics simulations at 300 K it was found that the same NTs can store only one H_2 molecule. On the other hand, the NT CBN(4,2) can store two H_2 molecules in both cases. Although the NTs CBN(7,0) and C(7,0) have the same length and radius, $\text{H}_2@\text{C}(7,0)$ have higher total energy value than that of $\text{H}_2@\text{CBN}(7,0)$. Therefore, we can say that the substitutional boron-nitrite doping reduces the total energy value in CNTs. Figures 4.7-4.9 give, respectively, potential, kinetic, and total energy change of NTs at 300 K that energy values reduce to a constant value in graphs from 0 to 1 picosecond.

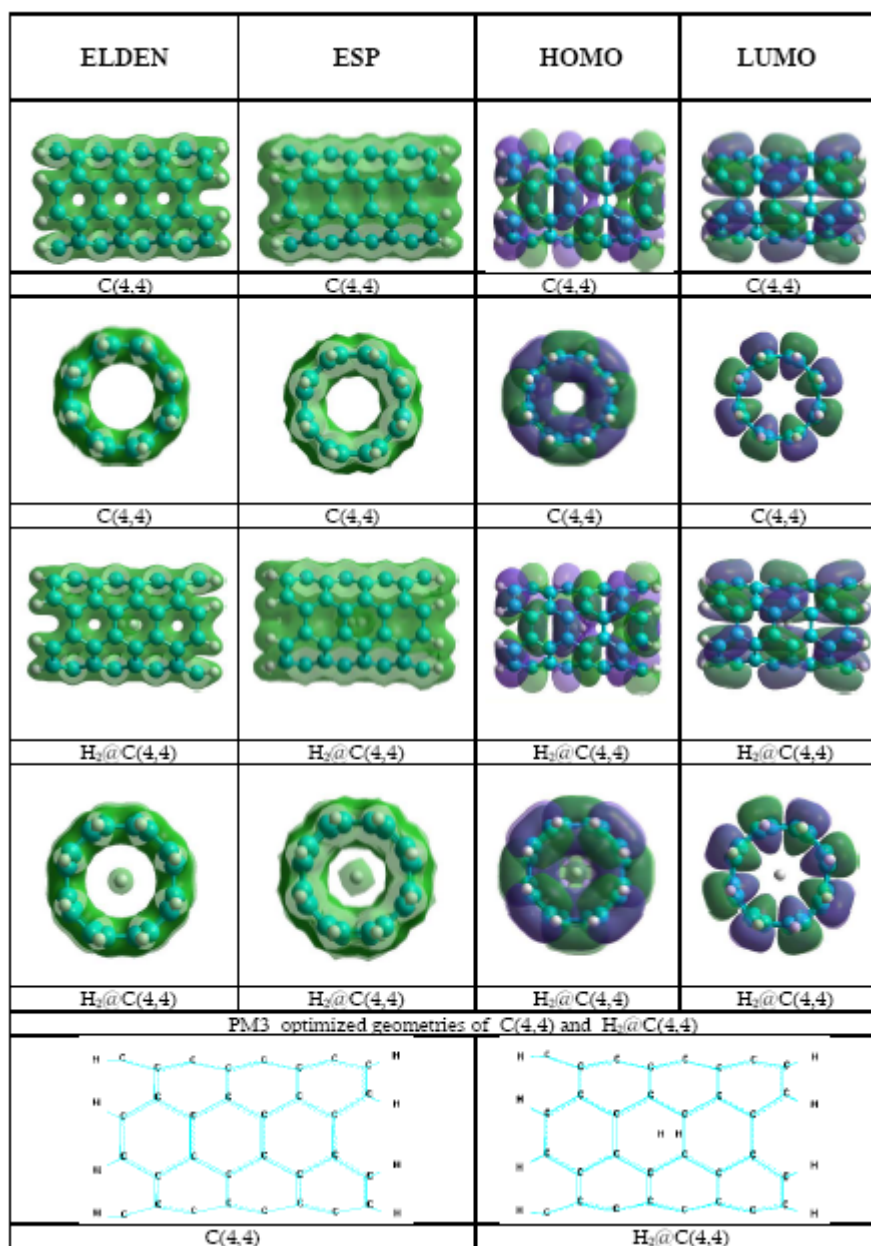


Figure 4.1: 3D HOMO, LUMO, ESP and ED plots of C(4,4), H₂@C(4,4) obtained from DFT/B3LYP/3-21G results and their optimized geometries obtained from PM3 results.

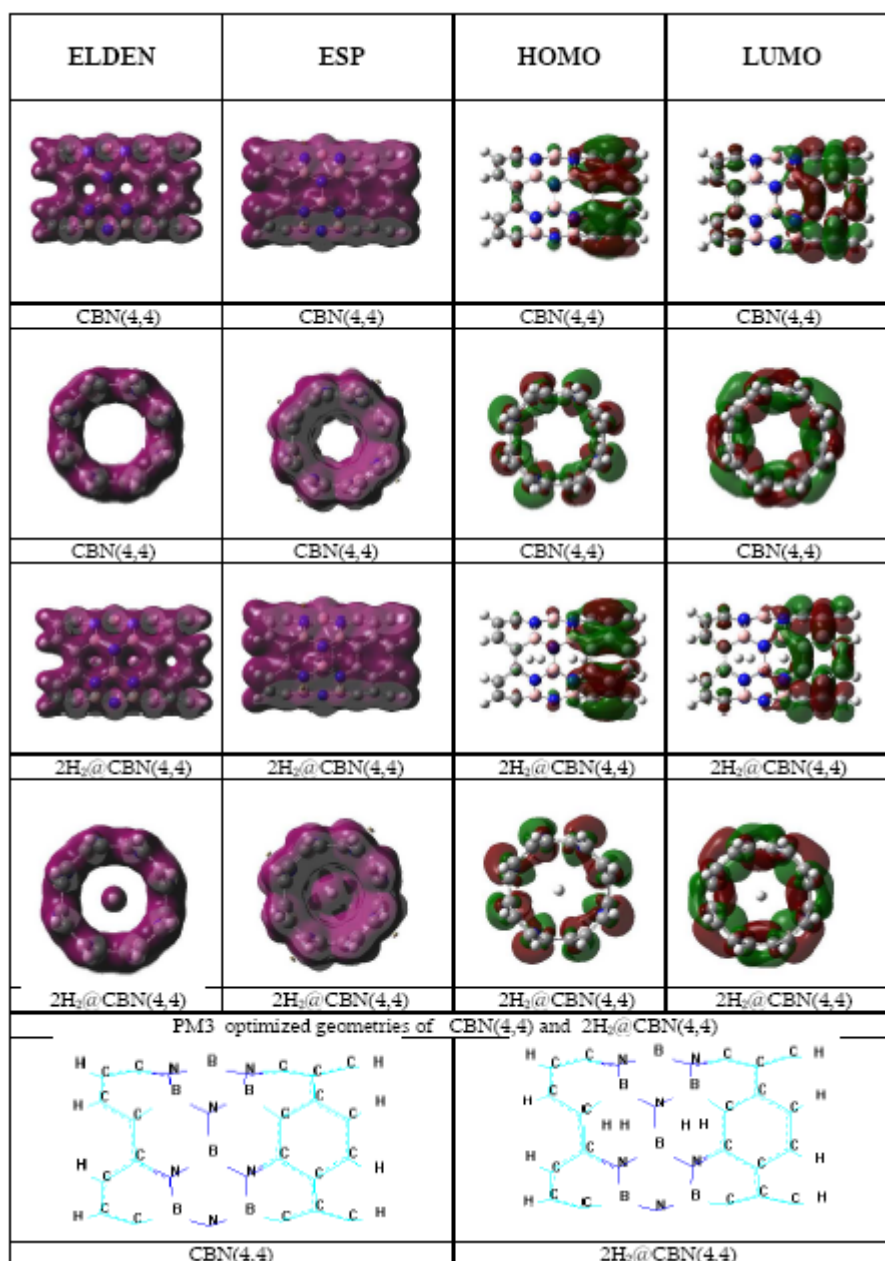


Figure 4.2: 3D HOMO, LUMO, ESP and ED plots of CBN(4,4), 2H₂@CBN(4,4) obtained from DFT/B3LYP/3-21G results and their optimized geometries obtained from PM3 results.

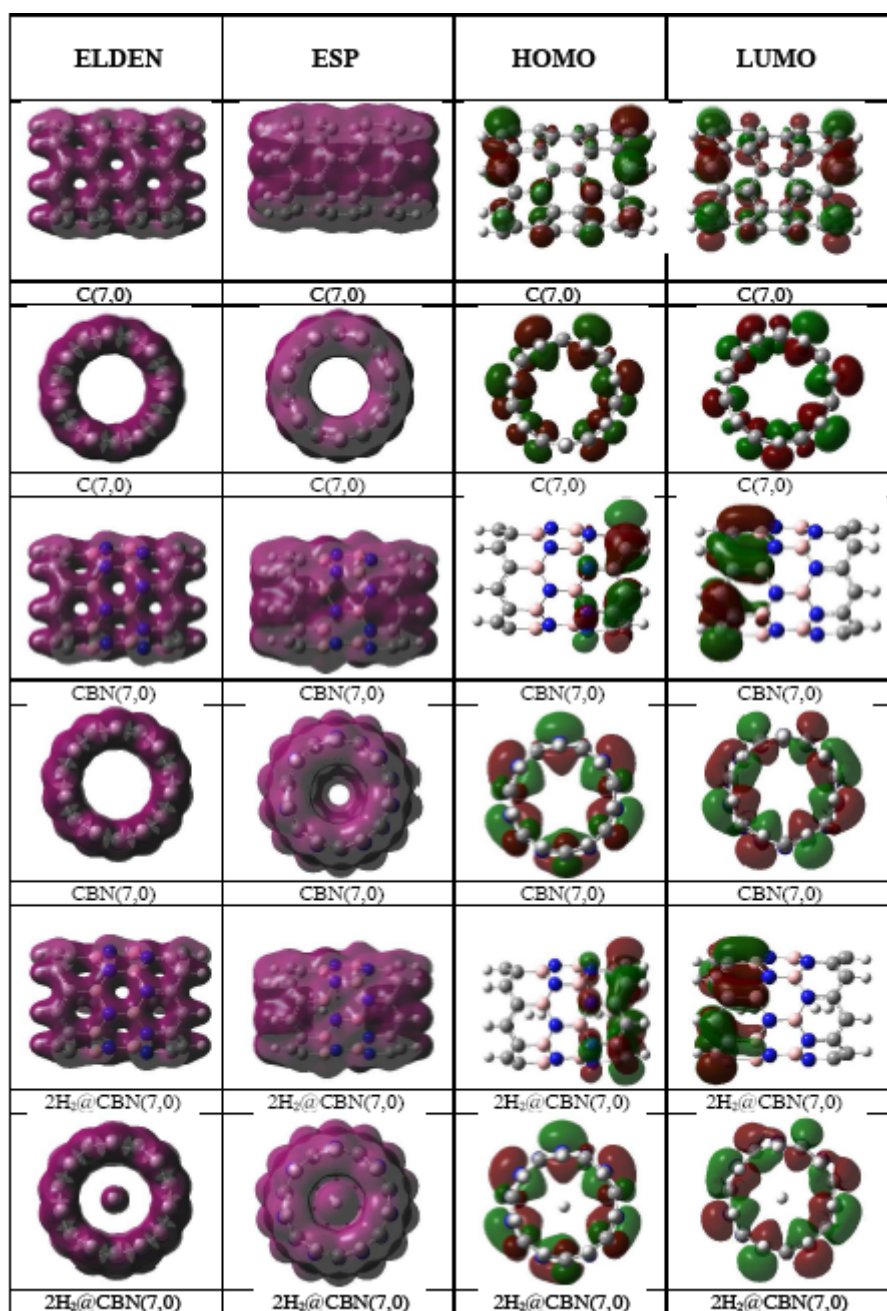


Figure 4.3: 3D HOMO, LUMO, ESP and ED plots of C(7,0), CBN(7,0), 2H₂@C(7,0) obtained from DFT/B3LYP/3-21G results.

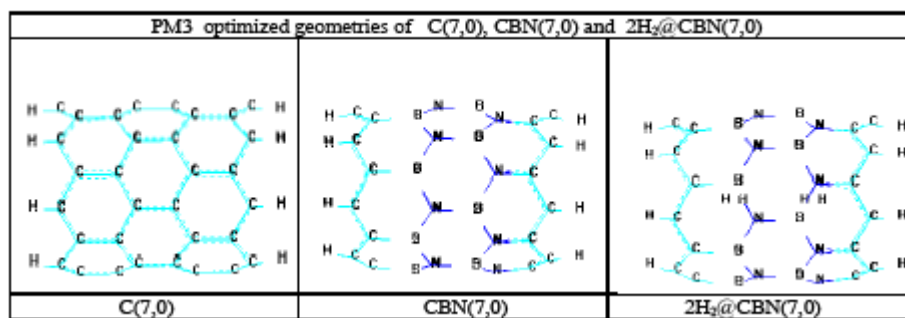


Figure 4.4: C(7,0), CBN(7,0) and 2H₂@C(7,0) optimized geometries obtained from PM3 results.

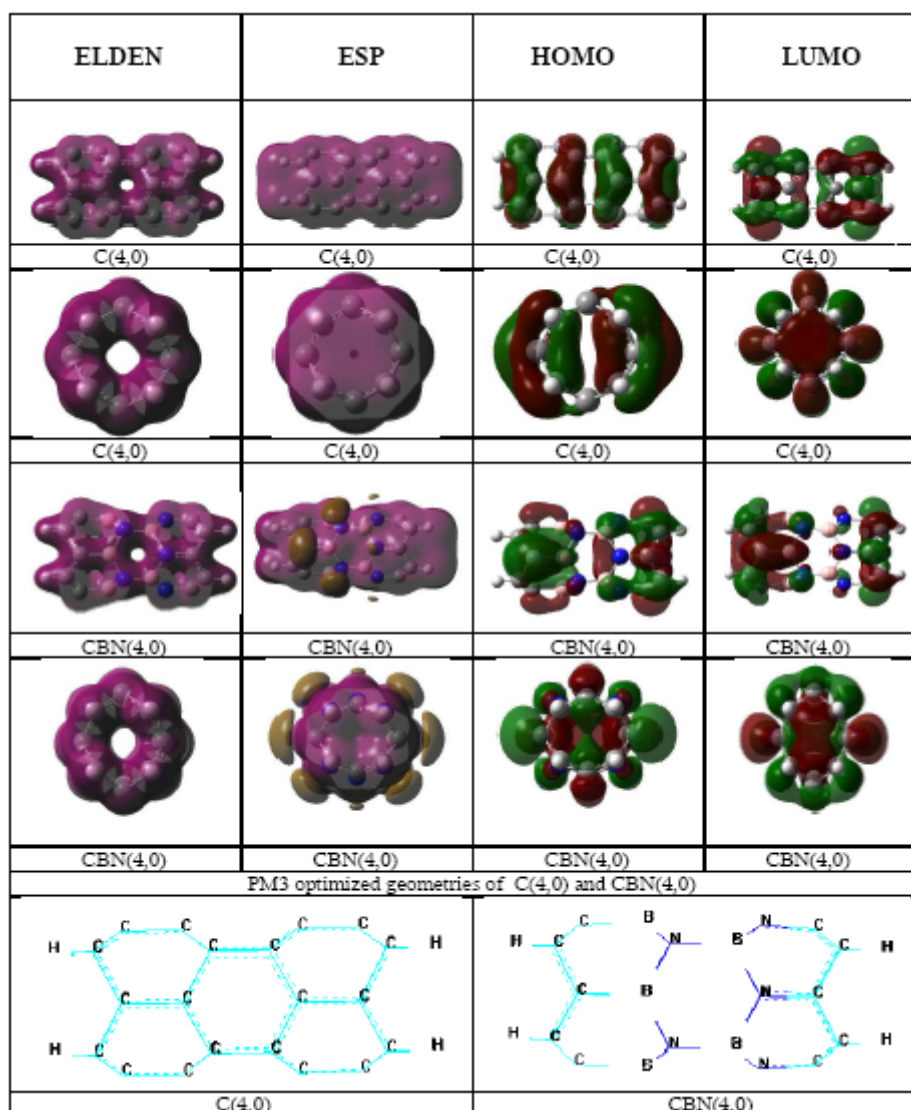


Figure 4.5: 3D HOMO, LUMO, ESP and ED plots of C(4,0), CBN(4,0) obtained from DFT/B3LYP/3-21G results and their optimized geometries obtained from PM3 results.

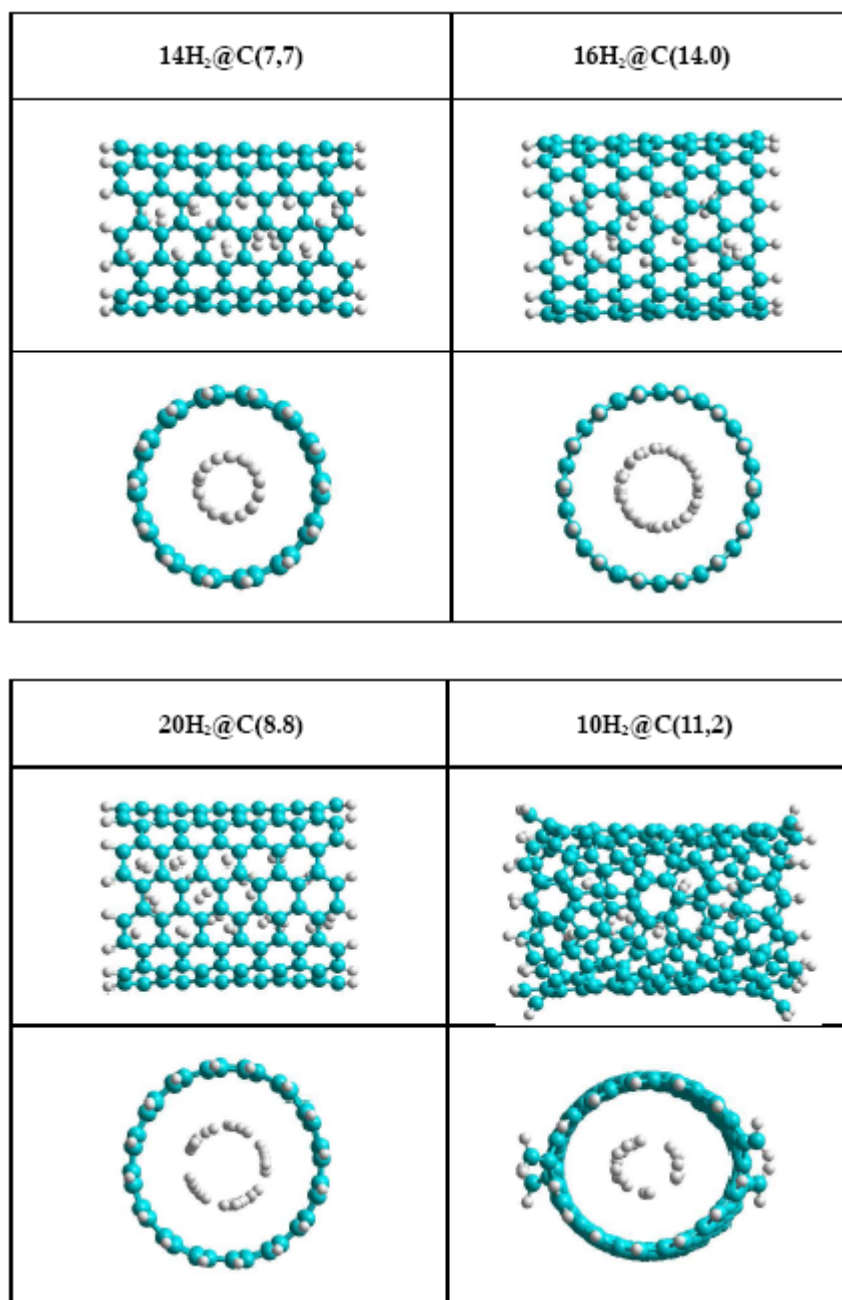


Figure 4.6: Hydrogen distribution inside of the carbon nanotubes having more than 9H₂.

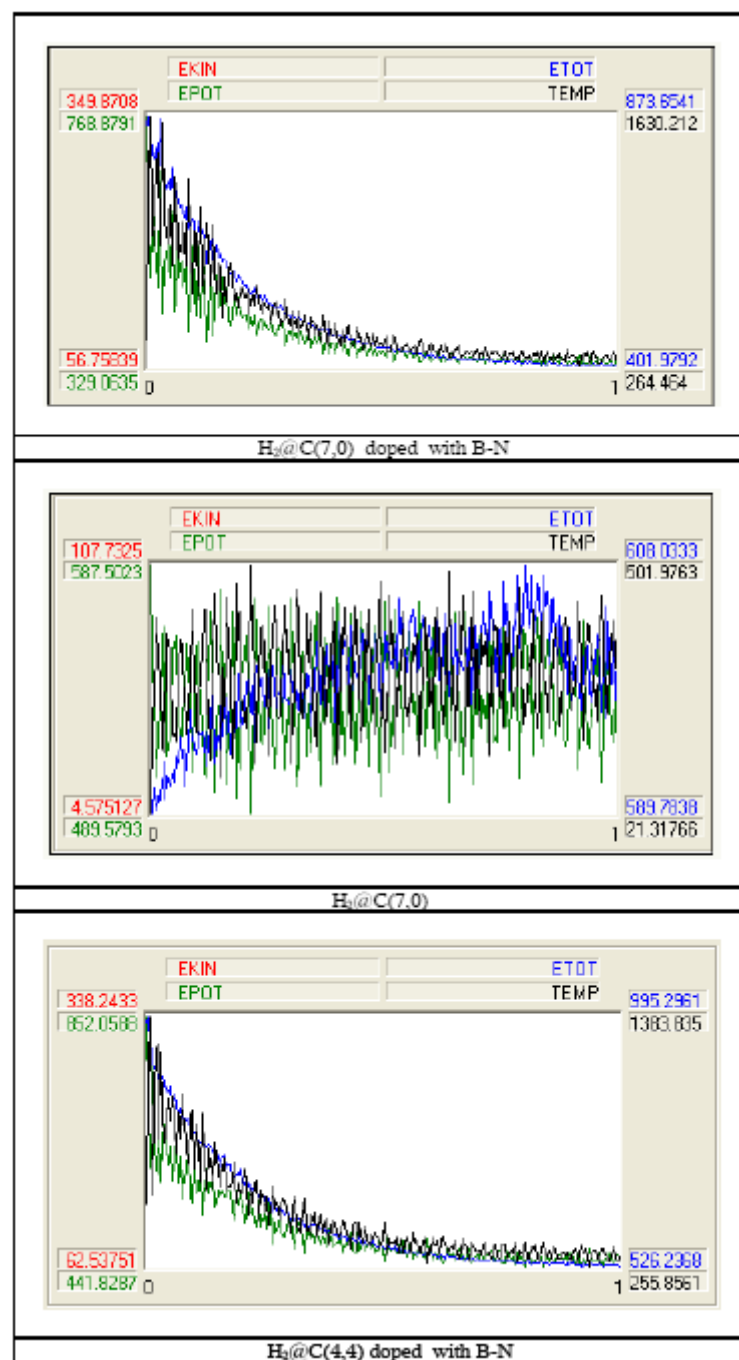


Figure 4.7: Molecular dynamics averages to be taken between 0 and 1 pico second for $H_2@CBN(7,0)$, $H_2@C(7,0)$, and $H_2@C(4,4)$ systems.

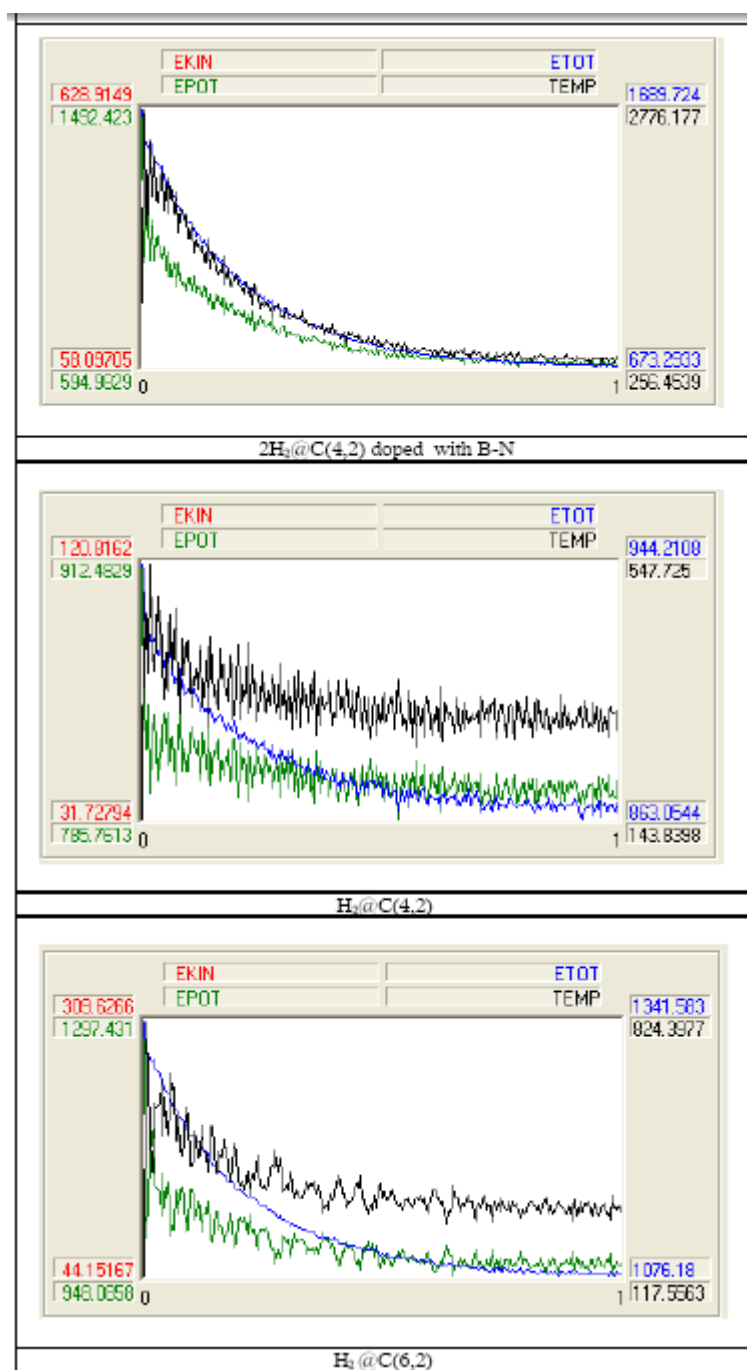


Figure 4.8: Molecular dynamics averages to be taken between 0 and 1 pico second for $2H_2@CBN(4,2)$, $H_2@C(4,2)$, and $H_2@C(6,2)$ systems.

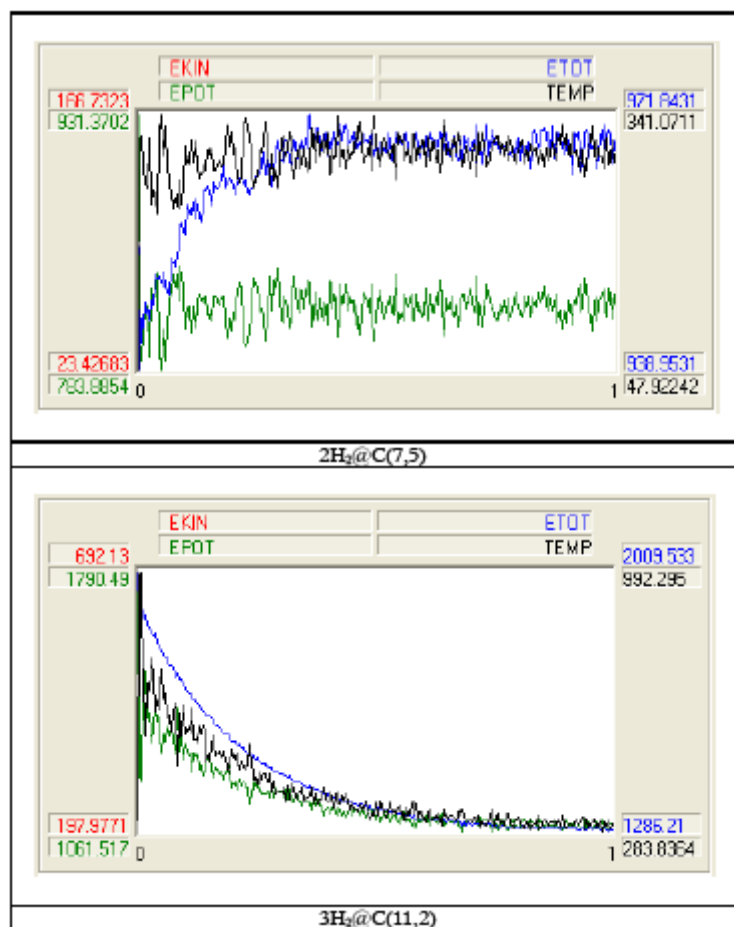


Figure 4.9: Molecular dynamics averages to be taken between 0 and 1 pico second for 2H₂@C(7,5), and 3H₂@C(11,2) systems.

4.2.1 DFT Study Results for BN Doped Coronene Model

The binding energies of stored hydrogen were calculated from DFT calculations. A stable system is defined to have negative binding energy in this study. The binding energy calculated per H₂ molecule for 7H₂@ B₃N₃C₁₈H₁₂ (in kcal/mol) is defined as follows:

$$\Delta E_{bind} = E(7H_2@ B_3N_3C_{18}H_{12}) - E(H_2) - E(6H_2@ B_3N_3C_{18}H_{12})$$

where $E(7H_2@ B_3N_3C_{18}H_{12})$, $E(6H_2@ B_3N_3C_{18}H_{12})$, and $E(H_2)$ are the total energies of fully optimized 7H₂@ B₃N₃C₁₈H₁₂ structure, 6H₂@ B₃N₃C₁₈H₁₂ structure, the hydrogen molecule, respectively. Calculations shows that E_{bind} per H₂ molecule is -0.41 eV for 7H₂@ B₃N₃C₁₈H₁₂ structure that is a stable system. Also, we obtained 4.45 wt % H storage for 7H₂@ B₃N₃C₁₈H₁₂ structure. In addition to this work, we put another 7H₂ molecules on the system of B₃N₃C₁₈H₁₂. When 7H₂ molecules were placed to down position of B₃N₃C₁₈H₁₂, we observed that 7H₂ molecules (up position) and 7H₂ molecules (down position) were adsorbed by the system of B₃N₃C₁₈H₁₂ from PM3 calculation ; in other words, when the system of B₃N₃C₁₈H₁₂ adsorbed 14H₂ molecules, it can be stable. E_{bind} per H₂ molecule calculated from the same way is -0.18 eV for 14H₂@ B₃N₃C₁₈H₁₂ structure and 8.53 wt % H storage for 14H₂@ B₃N₃C₁₈H₁₂ structure was obtained from PM3 calculation. According to the electronic structures of B₃N₃C₁₈H₁₂ and 7H₂@B₃N₃C₁₈H₁₂, 3D plots of the highest occupied molecular orbital (HOMO), the lowest unoccupied molecular orbital (LUMO), electrostatic potential (ESP), and electron density (ELDEN) figures are shown in Figure 4.10.

ESP and ED plots for the systems show a uniform distribution. From ESP figures, positive ESP plot for $B_3N_3C_{18}H_{12}$ and negative ESP plot for $7H_2@B_3N_3C_{18}H_{12}$ show a homogeneous distribution.

Table 4.7 shows the number of atoms in the systems under studying. Also, it gives total energy values calculated from geometric optimization using molecular mechanics method considering MM+ force field. Table 4.8 gives energies of the systems obtained from PM3 calculation for $B_3N_3C_{18}H_{12}$, $6H_2@B_3N_3C_{18}H_{12}$, $7H_2@B_3N_3C_{18}H_{12}$. It can be seen from Table 4.9, HOMO-LUMO gap for $7H_2@B_3N_3C_{18}H_{12}$, a stable system, is 3.30 eV. Also, while formation of $6H_2@B_3N_3C_{18}H_{12}$ and $7H_2@B_3N_3C_{18}H_{12}$ is exothermic, $B_3N_3C_{18}H_{12}$ is endothermic. The calculated dipole moment values are also shown in Table 4.9. In addition to this, Table 4.10 gives energies of the systems obtained from PM3 calculation for $13H_2@B_3N_3C_{18}H_{12}$, $14H_2@B_3N_3C_{18}H_{12}$. Figure 4.11 shows PM3 optimized geometries of the systems. It can be observed that the distance between hydrogen molecules and the system of $B_3N_3C_{18}H_{12}$ is about 3.16Å which is a suitable distance to store H_2 molecules. Figure 4.12 gives some information about HOMO, LUMO, HUMO, LOMO.

4.2.2 Molecular Dynamics Simulation Study Results for BN Doped Coronene Model

Table 4.11 displays potential energy, kinetic energy, and total energy values of the systems under study. Molecular dynamics simulations were run under the constant temperature of 300K. Figure 4.13 shows molecular dynamics averages to be taken from 0 to 1 pico second. We observed that the systems under study is stable at the room temperature. During the molecular dynamics simulations, H_2 molecules were leaving from the system of $B_3N_3C_{18}H_{12}$ in the course of time, which means that BN doped coronene model can absorb H_2 molecules and desorb them at the room temperature.

Table 4.7: $7\text{H}_2@B_3N_3C_{18}H_{12}$ and $14\text{H}_2@B_3N_3C_{18}H_{12}$ calculated energies from geometry optimization using molecular mechanics method considering MM+ force field. R: radius in °A; L: length in °A; TE: total energy in kcal/mol.

Quantity	# atoms	TE
$7\text{H}_2@B_3N_3C_{18}H_{12}$	3B, 3N, 18C	10.42
$14\text{H}_2@B_3N_3C_{18}H_{12}$	3B, 3N, 18C	0.52

Table 4.8: Calculated energies (in kcal/mol) from PM3, for $B_3N_3C_{18}H_{12}$, $6\text{H}_2@B_3N_3C_{18}H_{12}$, $7\text{H}_2@B_3N_3C_{18}H_{12}$.

Quantity	$B_3N_3C_{18}H_{12}$	$6\text{H}_2@B_3N_3C_{18}H_{12}$	$7\text{H}_2@B_3N_3C_{18}H_{12}$
Total Energy	-69433.29	-74462.77	-79492.17
Binding Energy	-4395.46	-5204.26	-6013.00
Isolated Atomic Energy	-65037.83	-69258.50	-73479.17
Electronic Energy	-550634.16	-666500.18	-791523.08
Core-Core Interaction	481200.86	592037.42	712030.91
Heat of Formation	51.88	-27.49	-106.80

Table 4.9: Calculated total energy (ET in kcal/mol), HOMO-LUMO gap (ΔE in eV), dipole moment (μ in Debye), binding energy per H_2 (ΔE_b , in eV) (from DFT/B3LYP/3-21G calculations (*)) and binding energy (E_b in kcal/mol), heat of formation (HoF in kcal/mol) (from PM3 calculations (**)).

System	ET(*)	ΔE (*)	μ (*)	ΔE_b (*)	E_b (**)	HoF(**)
H_2	-724.13	8.05	0.00	-	-718.95	-11.79
$B_3N_3C_{18}H_{12}$	-581377.28	3.30	0.01	-	-69433.29	51.88
$6H_2@ B_3N_3C_{18}H_{12}$	-585717.57	3.28	0.40	-	-73743.33	-15.22
$7H_2@ B_3N_3C_{18}H_{12}$	-586451.06	3.30	0.25	-0.41	-74462.77	-27.49

Table 4.10: Calculated energies (in kcal/mol) from PM3, for $13H_2@B_3N_3C_{18}H_{12}$, $14H_2@ B_3N_3C_{18}H_{12}$. Binding energy per H_2 (ΔE_b , in eV) (from PM3 calculation).

Quantity	$13H_2@ B_3N_3C_{18}H_{12}$	$14H_2@ B_3N_3C_{18}H_{12}$
Total Energy	-78771.01	-79494.17
Binding Energy	-5896.79	-6013.00
Isolated Atomic Energy	-72876.21	-73479.17
Electronic Energy	-772815.05	-791523.08
Core-Core Interaction	694042.04	712030.91
Heat of Formation	-94.79	-106.80
ΔE_b	---	-0.18

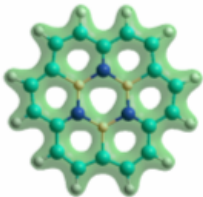
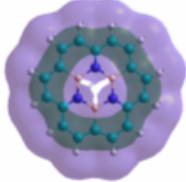
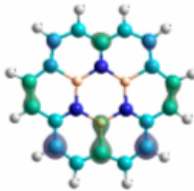
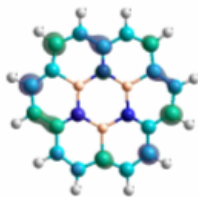
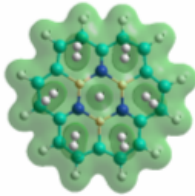
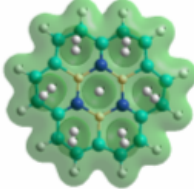
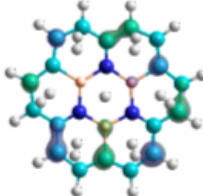
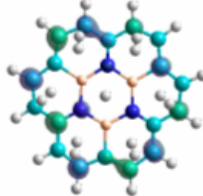
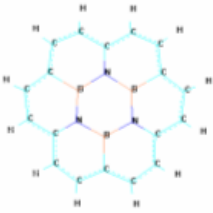
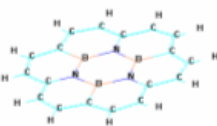
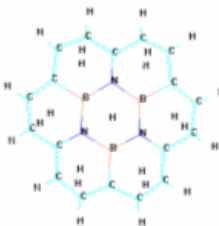
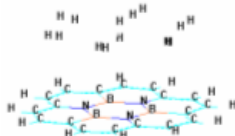
Charge Density	Electrostatic Potential	HOMO	LUMO
			
$B_3N_3C_{18}H_{12}$	$B_3N_3C_{18}H_{12}$	$B_3N_3C_{18}H_{12}$	$B_3N_3C_{18}H_{12}$
			
$7H_2@B_3N_3C_{18}H_{12}$	$7H_2@B_3N_3C_{18}H_{12}$	$7H_2@B_3N_3C_{18}H_{12}$	$7H_2@B_3N_3C_{18}H_{12}$
			
PM3 optimized geometries of $B_3N_3C_{18}H_{12}$		PM3 optimized geometries of $7H_2@B_3N_3C_{18}H_{12}$	

Figure 4.10: 3D HOMO, LUMO, ESP and ED plots of $B_3N_3C_{18}H_{12}$ and $7H_2@B_3N_3C_{18}H_{12}$ obtained from DFT/B3LYP/3-21G results and their optimized geometries obtained from PM3 results.

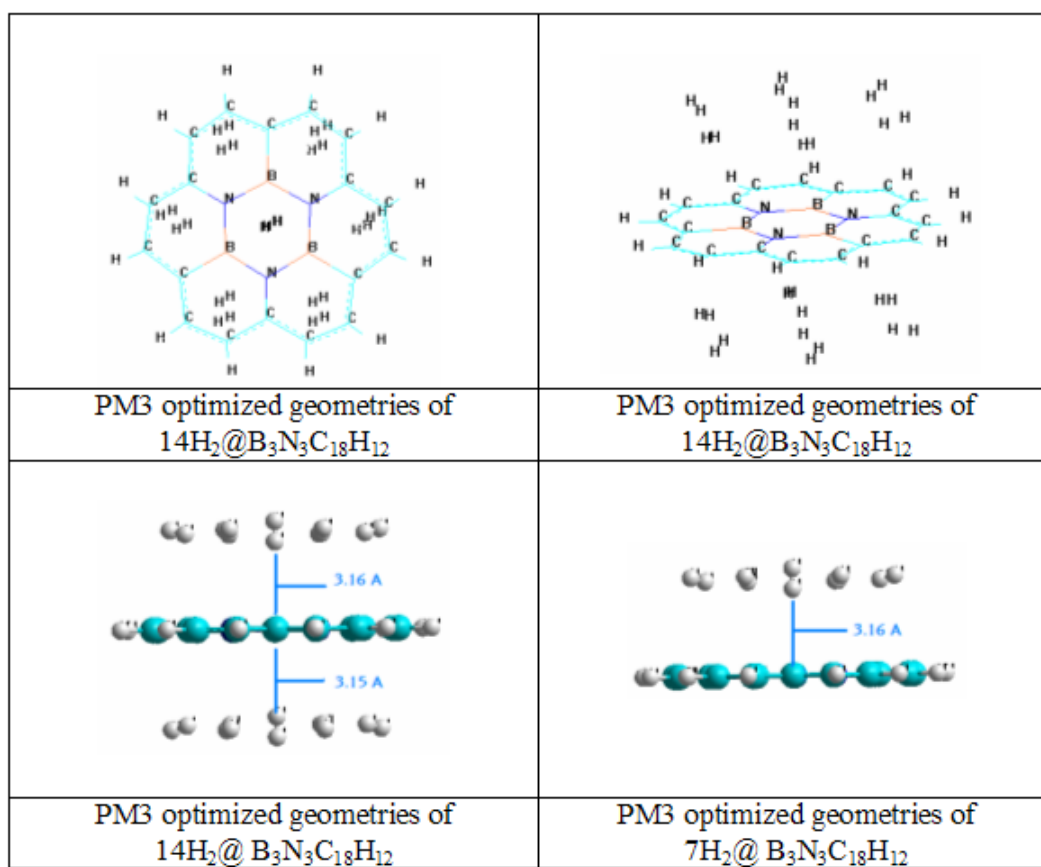


Figure 4.11: $7\text{H}_2@B_3N_3C_{18}H_{12}$ and $14\text{H}_2@B_3N_3C_{18}H_{12}$ optimized geometries obtained from PM3 results. The distance from $B_3N_3C_{18}H_{12}$ to 7H_2 is about 3.16Å.

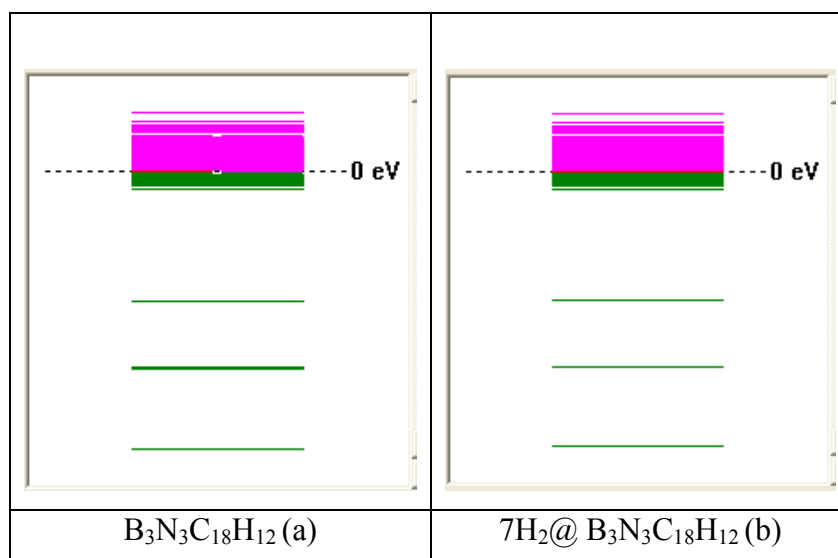


Figure 4.12: Molecular orbital eigenvalue spectra of the BN doped coronene model considered (DFT results). (a) HOMO: -4.928 eV; LUMO: -1.627 eV; HUMO: 80.098 eV; LOMO: -388.795 eV (b) HOMO: -4.940 eV; LUMO: -1.639 eV; HUMO: 80.849 eV; LOMO: -388.858 eV.

Table 4.11: Calculated energies from molecular dynamics with constant temperature 300K using molecular mechanics method considering MM+ force field for C(n,m) nanotubes. PE: potential energy in kcal/mol; KE: kinetic energy in kcal/mol; TE: total energy in kcal/mol; T: temperature in Kelvin.

Quantity	PE	KE	TE	T
7H ₂ @ B ₃ N ₃ C ₁₈ H ₁₂	40.26	51.53	91.79	345.77
14 H ₂ @ B ₃ N ₃ C ₁₈ H ₁₂	41.94	65.94	107.89	345.66

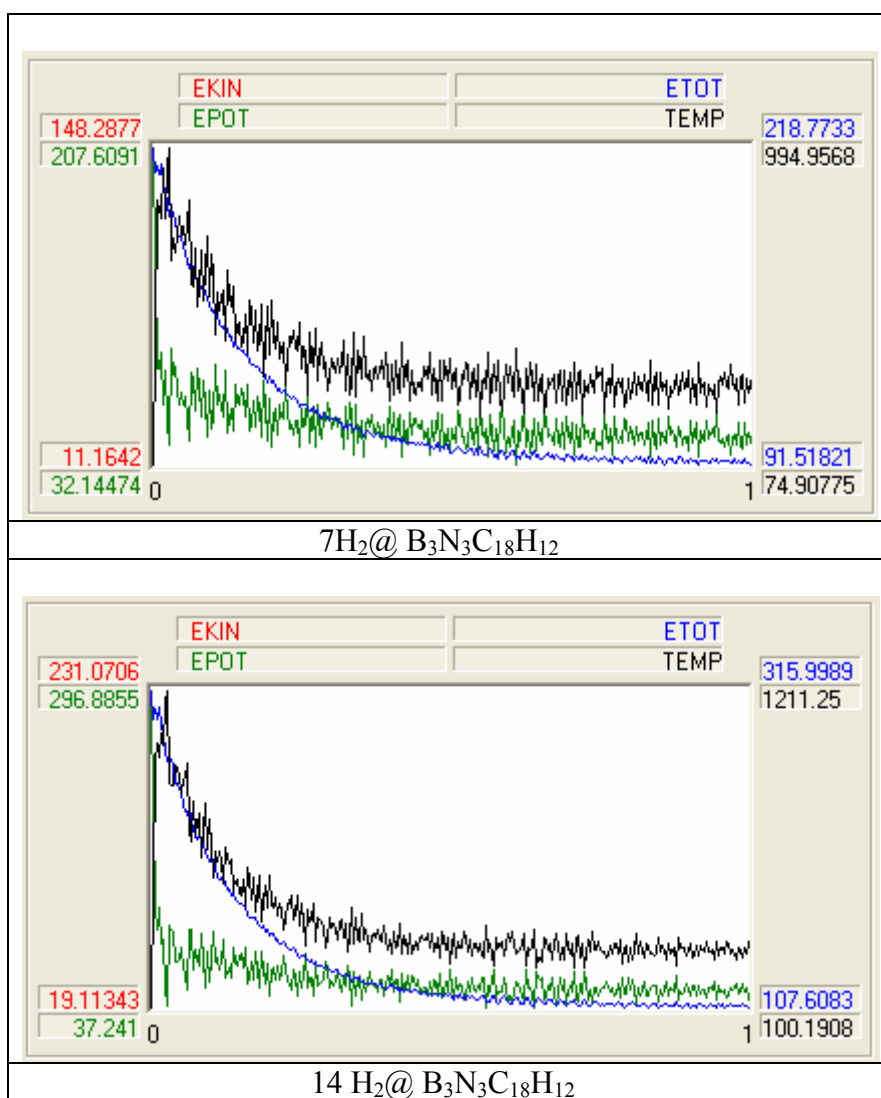


Figure 4.13: Molecular dynamics averages to be taken between 0 and 1 picosecond for $7\text{H}_2@ \text{B}_3\text{N}_3\text{C}_{18}\text{H}_{12}$ and $14 \text{H}_2@ \text{B}_3\text{N}_3\text{C}_{18}\text{H}_{12}$ systems.

CHAPTER 5

CONCLUSIONS

We have presented DFT calculation results of hydrogen adsorption on the CNTs doped with BN and investigated bare and CNTs doped with BN of various lengths and radii. Enhancement of hydrogen storage capacity of carbon nanotubes via BN doping has been observed and the resulting configurations were found to be stable. We have observed that the H₂ storage capacity of CNTs increase with increasing radii. Table 4.5, C(7,0) and C(4,4) are able to store only one H₂ molecule, CBN(7,0) and CBN(4,4) having the same length and radius with C(7,0) and C(4,4) are able to store two H₂ molecules. The binding energies of H₂ calculated for CNTs substitutionally doped with BN are 0.27 eV and 0.54 eV which are suitable for absorption hydrogen molecules at room temperature and for desorption them upon heating. Furthermore, from molecular dynamics studies (Table 4.6), the hydrogen storage capacity reduces with increasing temperature. Moreover, again from molecular dynamics simulations, we observe that the molecular construction of CNTs doped with BN does not break with increasing temperature. Therefore, CNTs substitutionally doped with BN is more convenient to desorp hydrogen, and such systems can be considered as potential materials for hydrogen storage purposes.

Because of the hydrogen storage capacity, BN doped coronene model is a promising hydrogen storage system. We observed that $B_3N_3C_{18}H_{12}$ can store H_2 molecules both up position and down position of it. Also, hydrogen molecules have distributed on the system symmetrically. In addition, from MD simulations, it can be seen that the system of $B_3N_3C_{18}H_{12}$ is not breaking when it is heated.

REFERENCES

1. Züttel A., Hydrogen Storage Methods and Materials, *Naturwissenschaften* 91 (2004) 157-72
2. Li Zhou, Progress and Problems in Hydrogen Storage Methods, *Renewable and Sustainable Energy Reviews*, 9 (2005) 395-408
3. T.Nejat Veziroğlu and Frano Barbir, *Hydrogen Energy Technologies*, UNIDO, 1998
4. R. Ströbel, J. Garche, P.T. Moseley, L.Jörissen, G. Wolf, Hydrogen Storage by Carbon materials, *Journal of Power Sources* 159 (2006) 781-801
5. S. Brunauer, P.H. Emmett, E. Teller, *J. Am. Chem. Soc.* 60 (1938)309
6. N. Textier-Mandoki, J. Dentzer, T. Piquero, S. Saadallah, P. David, C. Vix-Guterl, *Carbon* 42 (2001) 2744.
7. J. P. Lu, J. Han, *Int. J. High Speed Electron. Syst.* 9 (1998) 101.
8. P. M. Ajayan, *Chem. Rev.* 99 (1999) 1787.
9. H. W. Kroto, J. R. Heath, S. C. O' Brien, R. F. Curl, and R. E. Smalley, *Nature* 318 (1985) 162 .

10. R. Saito, G. Dresselhaus, M. S. Dresselhaus, Imperial College Press, Singapore, 1998.
11. S. Iijima, *Nature* 354 (1991) 56.
12. M. Dresselhaus, G. Dresselhaus, P. Eklund, R. Saito, *Phys. World* 11 (1998) (1) (Article 9).
13. R. Strbel, J. Garche, P.T. Moseley, L. Jrisen, G. Wolf, *Journal of Power Sources* 159 (2006) 781-801.
14. Andreas Zttel, *Naturwissenschaften* 91 (2004) 157-172.
15. W. Kohn, L.J. Sham, *Phys. Rev.* 140 (1965) A1133.
16. N.L. Allinger, *J. Am. Chem. Soc.* 99 (1977) 8127.
17. M. J. S. Dewar, E.G. Zoebish, E.F. Healey, J.J.P. Stewart, *J. Am. Chem. Soc*
18. Dillon AC, Jones KM, Bekkedahl TA, Kiang CH, Bethune DS, Heben MJ. Storage of hydrogen in single-walled carbon nanotubes. *Nature* 386 (1997) 377–9.
19. Dillon AC, Gennett T, Alleman JL, Jones KM, Parilla PA, Heben MJ. Carbon nanotube materials for hydrogen storage. *Proceedings of the 1999 U.S. DOE hydrogen program review, vol. II*
20. Liu C, Fan YY, Liu M, Cong HT, Cheng HM, Dresselhaus MS. Hydrogen storage in single-walled carbon nanotubes at room temperature. *Science* 1999;286(5442):1127–9.

21. Dillon AC, Gennett T, Alleman JL, Jones KM, Parilla PA, Heben MJ. Carbon nanotube materials for hydrogen storage. Proceedings of the 2000 U.S. DOE hydrogen program review, vol. II
22. Tibbets GG, Meisner GP, Olk CH. Hydrogen storage capacity of carbon nanotubes, filaments and vapor-grown fibers. Carbon 39 (2001) 2291–301.
23. Hirscher M, Becher M, Haluska M, Dettlaff-Weglikowska U, Quintel A, Duesberg GS. et al. Hydrogen storage in sonicated carbon materials. Appl Phys A 72(2) (2001) 129–32.
24. Nishimiya N, Ishigaki K, Takikawa H, Ikeda M, Hibi Y, Sakakibara T. et al. Hydrogen sorption by single-walled carbon nanotubes prepared by a torch arc method. J Alloys Comp 339 (2002) 275–82.
25. Hirscher M, Becher M, Haluska M, Quintel A, Skakalova V, Choi Y-M. et al. Hydrogen storage in carbon nanostructures. J Alloys Comp 332 (2002) 654–8.
26. Liu C, Yang QH, Tong Y, Cong HT, Cheng HM. Volumetric hydrogen storage in single-walled carbon nanotubes. Appl Phys Lett 80(13) (2002)2389–91.
27. Fonseca A, Pierard N, Tollis S, Bister G, Konya Z, Nagaraju N. et al. Hydrogen storage in carbon nanotubes produced by CVD. J Phys IV 12 (2002) 129–37.
28. Shiraishi M, Takenobu T, Ata M. Gas–solid interactions in the hydrogen/single-walled carbon nanotube system. Chem Phys Lett 367(2003) 633–6.

29. David P, Piquero T, Metenier K, Pierre Y, Demoment J, Lecas-Hardit A. Hydrogen adsorption in carbon materials. Proceedings of the first European hydrogen energy conference, Grenoble, 2003.
30. Kajiura H, Tsutsui S, Kadono K, Kakuta M, Ata M, Murakami Y. Hydrogen storage capacity of commercially available carbon materials at room temperature. *Appl Phys Lett* 82 (2003) 1105–7.
31. Li X, Zhu H, Xu C, Mao Z, Wu D. Measuring hydrogen storage capacity of carbon nanotubes by tangent-mass method. *Int J Hydrogen Energy* 28(11) (2003) 1251–3.
32. Smith MR, Bittner EW, Shi W, Johnson JK, Bockrath BC. Chemical activation of single-walled carbon nanotubes for hydrogen adsorption. *J Phys Chem B* 107 (2003) 3752–60.
33. Gao H, Wu B, Li JT, Wu GT, Lin JY, Wu K. et al. Hydrogen adsorption of open-tipped insufficiently graphitized multiwalled carbon nanotubes. *Appl Phys Lett* 83(16) (2003) 3389–91.
34. Gundiah G, Govindaraj A, Rajalakshmi N, Dhathathereyan KS, Rao CNR. Hydrogen storage in carbon nanotubes and related materials. *J Mater Chem* 13 (2003) 209–13.
35. Tarasov BP, Maehlen JP, Lototsky MV, Muradyan VE, Yartys VA. Hydrogen sorption properties of arc generated single-wall carbon nanotubes. *J Alloys Comp* 356–357 (2003) 510–4.

36. Lawrence J, Xu G. High pressure saturation of hydrogen stored by single-wall carbon nanotubes. *Appl Phys Lett* 84(6) (2004) 918–20.
37. Takagi H, Hatori H, Soneda Y, Yoshizawa N, Yamada Y. Adsorptive hydrogen storage in carbon and porous materials. *Mat Sci Eng B* 108 (2004) 143–7.
38. Poirier E, Chahine R, Bénard P, Cossement D, Lafi L, Mélançon E, Bose TK. et al. Storage of hydrogen on single-walled carbon nanotubes and other carbon structures. *Appl Phys A* 78 (2004) 961–7.
39. Ansón A, Jagiello J, Parra JB, Sanjuán ML, Benito AM, Wolfgang KM. et al. Porosity, surface area, surface energy, and hydrogen adsorption in nanostructured carbons. *J Phys Chem B* 108(40) (2004) 15820–6.
40. Ritschel M, Uhlemann M, Gutfleisch O, Leonhardt A, Graff A, Täschner Ch et al. Hydrogen storage in different carbon nanostructures. *Appl Phys Lett* 80(16) (2002) 2985–7.
41. Luxembourg D, Flamant G, Guillot A, Laplaze D. Hydrogen storage in solar produced single-walled carbon nanotubes. *Mat Sci Eng B* 108 (2004) 114–9.
42. D. Luxembourg, G. Flamant, E. Beche, J. Sans, J. Giral, V. Goetz,
Hydrogen storage capacity at high pressure of raw and purified single wall carbon nanotubes produced with a solar reactor, *International Journal of Hydrogen Energy*, 2006.
43. A.C. Dillon, K.M. Jones, T.A. Bekkedahl, C.H. Kiang, D.S. Bethune, M.J. Heben, *Nature* 386 (1997) 377.

44. A.C. Dillon, T. Gennet, J.L. Alleman, K.M. Jones, P.A. Parilla, M.J. Heben, DOE Hydrogen Program, FY 1999 Progress Report.
45. C. Liu, Y.Y. Fan, M. Liu, H.T. Cong, H.M. Cheng, M. Dresselhaus, *Science* 286 (1999) 1127.
46. C. Liu, Q.H. Yang, Y. Tong, H.T. Cong, H.M. Cheng, *Appl. Phys. Lett.* 80 (2002) 2389.
47. X. Chen, U. Detlaff-Weglikowska, M. Haluska, M. Hulman, S. Roth, M. Hirscher, M. Becher, *Mater. Res. Soc. Symp. Proc.* 706 (2002) 295.
48. Y. Ye, C.C. Ahn, C. Whitam, B. Fultz, L. Liu, A.G. Rinzler, D. Colbert, K.A. Smith, R.E. Smalley, *J. Appl. Phys. Lett.* 74 (1999) 2307.
49. X.B. Wu, P. Chen, J. Lin, K.L. Tan, *Int. J. Hydrogen Energy* 25 (1999) 261.
50. M.R. Smith, E.W. Bittner, W. Shi, J.K. Johnson, B.C. Bockrath, *J. Phys. Chem. B* 107 (2003) 3752.
51. A.C. Dillon, T. Gennet, J.L. Alleman, K.M. Jones, P.A. Parilla, M. Heben, DOE Hydrogen Program, FY 2000 Progress Report.
52. M.Hirscher, M.Becher, M.Haluska, A.Quintel, U.Detlaff- Weglikowska, G.S. Duesberg, Y.M. Coi, P. Downes, M. Hulman, S. Roth, I. Stepanek, P. Bernier, *Appl. Phys. A* 72 (2001) 129.

53. M. Hirscher, M. Becher, M. Haluska, A. Quintel, V. Skakalova, Y.M. Coi, U. Detlaff-Weglikowska, S. Roth, I. Stepanek, P. Bernier, A. Leonhardt, J. Fink, J. Alloys Compd. 330–332 (2001) 654.
54. R. Zidan, A.M. Rao, DOE Hydrogen Program, FY 2002 Progress Report.
55. P. Chen, X. Wu, J. Lin, K.L. Tan, Science 285 (1999) 91.
56. R.T. Yang, Carbon 38 (2000) 623.
57. F.E. Pinkerton, B.G. Wicke, C.H. Olk, G.G. Tibbetts, G.P. Meisner, M.S. Meyer, J.F. Herbst, J. Phys. Chem. B 104 (2000) 9460.
58. M. Ritschel, M. Uhlemann, O. Gutfleisch, A. Leonhardt, A. Graff, C. Taschner, J. Fink, Appl. Phys. Lett. 80 (2002) 2985.
59. R.G. Ding, G.Q. Lu, Z.F. Lan, unpublished results, 2003.
60. C.D.W. Adu, G.U. Sumanasekara, B.K. Pradhan, H.E. Romero, P.C. Eklund, Chem. Phys. Lett. 337 (2001) 31.
61. B.K. Pradhan, A. Harutyunyan, D. Stojkovic, P. Zhang, M.W. Cole, V. Crespi, H. Goto, J. Fujiwara, P.C. Eklund, Mater. Res. Soc. Symp. Proc. 706 (2002) 331.
62. H. Zhu, A. Cao, X. Li, C. Xu, Z. Mao, D. Ruan, J. Liang, D. Wu, Appl. Surf. Sci. 178 (2001) 50.

63. A. Cao, H. Zhu, X. Zhang, X. Li, D. Ruan, C. Xu, B. Wei, L. Liang, D. Wu, *Chem. Phys. Lett.* 342 (2001) 510.
64. Y. Chen, D.T. Shaw, X.D. Bai, E.G. Wang, C. Lund, W.M. Lu, D.D.L. Chung, *Appl. Phys. Lett.* 78 (2001) 2128.
65. A. Badzian, T. Badzian, E. Breval, A. Piotrowski, *Thin Solid Films* 398–399 (2001) 170.
66. N. Nishimiya, H. Ishigaki, H. Takikawa, M. Ikeda, Y. Hibi, T. Sakak-ibara, A. Matsumoto, K. Tsutsumi, *J. Alloys Compd.* 339 (2002) 275.
67. G.G. Tibbetts, G.P. Meisner, C.H. Olk, *Carbon* 39 (2001) 2291.
68. A. Chambers, C. Park, R.T.K. Baker, N.M. Rodriguez, *J. Phys. Chem. B* 102 (1998) 4253.
69. R. Ströbel, J. Garche, P.T. Moseley, L. Jörisen, G. Wolf, *Hydrogen Storage by Carbon Materials, Journal of Power Sources* 159 (2006) 781-801
70. C.C. Ahn, Y. Ye, B.V. Ratnakumar, C. Witham, R.C. Bowman Jr., B. Fultz, *Appl. Phys. Lett.* 73 (1998) 3378.
71. D.J. Browning, M.L. Gerrard, J.B. Lakeman, I.M. Mellor, R.J. Mortimer, M.C. Turpin, in: Z.Q. Mao, T.N. Veziroglu (Eds.), *Hydrogen Energy Progress XIII, Proceedings of the 13th World Hydrogen Energy Conference, Beijing, June 11–15 (2000)* 554–559.
72. E. Poirier, R. Chahin, T.K. Bose, *Int. J. Hydrogen Energy* 26 (2001) 831.

73. M.A. de la Casa-Lillo, F. Lamari-Darkrim, D. Cazorla-Amoros, A. Linares-Solano, *J. Phys. Chem. B* 106 (2002) 10930.
74. J.Y. Hwang, S.H. Lee, K.S. Sim, J.W. Kim, *Synth. Met.* 126 (2002) 81.
75. M. Hirscher, M. Becher, *J. Nanosci. Nanotechnol.* 3 (2003) 3.
76. R. Strobel, L. Jorissen, T. Schliermann, V. Trapp, W. Schütz, K. Bohnhammel, G. Wolf, J. Garce, *J. Power Sources* 84 (1999) 221.
77. B.K. Gupta, O.N. Srivastava, *Int. J. Hydrogen Energy* 25 (2000) 825.
78. B.K. Gupta, O.N. Srivastava, *Int. J. Hydrogen Energy* 26 (2001) 857.
79. Y.Y. Fan, B. Liao, M. Liu, Y.L. Wei, M.Q. Lu, H.M. Cheng, *Carbon* 37 (1999) 1649.
80. H.M. Cheng, C. Liu, Y.Y. Fan, F. Li, G. Su, L.L. He, M. Liu, *Z. Metallkd.* 91 (2000) 306.
81. C. Nutzenadel, A. Zuttel, D. Chartouni, L. Schlapbach, *Electrochem. Solid-State Lett.* 2 (1) (1999) 30.
82. K. Jurewicz, E. Frackowiak, F. Be'guin, *Electrochem. Solid-State Lett.* 4 (2001) A27.
83. X. Qin, X.P. Gao, H. Liu, H.T. Yuan, D.Y. Yan, W.L. Gong, D.Y. Song, *Electrochem. Solid-State Lett.* 3 (2000) 532.

84. S.M. Lee, K.S. Park, Y.C. Choi, Y.S. Park, J.M. Bok, D.J. Bae, K.S. Nahm, Y.G. Choi, S.Ch. Yu, N. Kim, T. Frauenheim, Y.H. Lee, *Synth. Met.* 113 (2000) 209.
85. N. Rajalakshmi, K.S. Dhathathreyan, A. Govindaraj, B.C. Satishkumar, *Electrochim. Acta* 45 (2000) 4511.
86. H.S. Youn, H. Ryu, T.H. Cho, W.K. Choi, *Int. J. Hydrogen Energy* 27 (2002) 937.
87. G. Dai, M. Liu, D. Chen, P. Hou, Y. Tong, H.M. Cheng, *Electrochem. Solid-State Lett.* 5 (2002) E13.
88. X.P. Gao, Y. Lan, G.L. Pan, F. Wu, J.Q. Qu, D.Y. Song, P.W. Shen, *Electrochem. Solid-State Lett.* 4 (2001) A173.
89. X. Yan, X. Gao, Y. Li, Z. Liu, F. Wu, Y. Shen, D. Song, *Chem. Phys. Lett.* 372 (2003) 336.
90. J.M. Skowronski, P. Scharff, N. Pfander, S.Cui, *Adv. Mater.* 15(1) (2003) 55.
91. X. Chen, Y. Zhang, X.P. Gao, G.L. Pan, X.Y. Jiang, J.Q. Qu, F. Wu, J. Yan, D.Y. Song, *Int. J. Hydrogen Energy* 29 (2004) 743.
92. J. Liu, Z. Mao, D. Hao, X. Xie, D. Wu, Presented at 204th ECS Meeting, Orlando, FL, October 12–16, 2003 (Abstract, 130).
93. G.P. Dai, C.Liu, M. Liu, M.Z. Wang, H.M. Cheng, *Nano Lett.* 2 (5) (2002) 503.

94. I. Lombardi, M. Bestetti, C. Mazzocchia, P.L. Cavallotti, U. Ducati, *Electrochem. Solid-State Lett.* 7 (2004) A115.
95. L.Z. Ouyang, F.X. Qin and M. Zhu, The hydrogen storage behavior of Mg₃La and Mg₃LaNi_{0.1}, *Scripta Materialia* 55 (2006) 1075–1077
96. R. Vijay, R. Sundaresan, M.P. Maiya, S. Srinivasa Murthy, Hydrogen storage properties of Mg–Cr₂O₃ nanocomposites: The role of catalyst distribution and grain size, *Journal of Alloys and Compounds* 424 (2006) 289–293
97. M. Jorda-Beneyto, F. Suares-García, D. Lozano-Castello, D. Cazorla-Amoros, A. Linares-Solano, Hydrogen storage on chemically activated carbons and carbon nanomaterials at high pressures, *Carbon* xxx (2006) xxx–xxx
98. Hao Gu, Yunfeng Zhu, Lique Li, Characterization of hydrogen storage properties of Mg-30 wt.% Ti_{1.0}V_{1.1}Mn_{0.9} composite, *Journal of Alloys and Compounds* 424 (2006) 382–387
99. Zhenian Li, Xiaopeng Liu, Lijun Jiang, Shumao Wang, Characterization of Mg–20 wt% Ni–Y hydrogen storage composite prepared by reactive mechanical alloying, *International Journal of Hydrogen Energy*
100. X.L. Wang, J.P. Tu, C.H. Wang, X.B. Zhang, C.P. Chen, X.B. Zhao, Hydrogen storage properties of nanocrystalline Mg–Ce/Ni composite, *Journal of Power Sources* 159 (2006) 163–166
101. James M. Blackman, John W. Patrick, Ana Arenillas, Wei Shi, Colin E. Snape, Activation of carbon nanofibres for hydrogen storage, *Carbon* 44 (2006) 1376–1385

102. Ming Au, Hydrogen storage properties of magnesium based nanostructured composite materials, *Materials Science and Engineering B* 117 (2005) 37–44
103. Li Qian, Lin Qin, Jiang Lijun, Kou-Chih Chou, Zhan Feng, Zheng Qiang, Wei Xiuying, Properties of hydrogen storage alloy $Mg_{2-x}Ag_xNi$ ($x=0.05, 0.1, 0.5$) by hydriding combustion synthesis, *Journal of Alloys and Compounds* 359 (2003) 128–132
104. A. R. Leach, *Molecular Modelling*, Longman, Essex, 1997.
105. Hypercube, Inc., Gainesville, FL, USA.
106. P. Fletcher, *Practical Methods of Optimization*, Wiley, New York, 1990.
107. A.D. Becke, *J. Chem. Phys.* 98 (1993)5648.
108. C. Lee, W. Yang, R.G. Parr, *Phys. Rev. B* 37 (1988)785.
109. W. J. Hehre, R.F. Stewart, J.A. Pople, *J. Chem. Phys.* 51 (1969) 2657.
110. M. J. Frisch, et al.,(2003), GAUSSIAN, Revision B.04, Gaussian, Inc., Pittsburgh, PA.
111. A.D. Becke, *J. Chem. Phys.* 98 (1993) 5648-5652.
112. C. Lee, W. Yang and R.G. Parr, *Phys. Rev. B* 37 (1988) 785-789.
113. B. Miehlich, A. Savin, H. Stoll and H. Preuss, *Chem. Phys. Lett.*, 157 (1988) 200-206.

114. I. Fleming, "Frontier orbitals and organic chemical reactions", John Wiley and Sons, New York, 1976.